Available online at www.sciencedirect.com

ScienceDirect

Geochimica et Cosmochimica Acta 258 (2019) 290–309

Geochimica et Cosmochimica Acta

www.elsevier.com/locate/gca

Hf-W chronology of ordinary chondrites

Jan L. Hellmann [a,*], Thomas S. Kruijer [a,b], James A. Van Orman [c], Knut Metzler [a], Thorsten Kleine [a]

[a] Institut für Planetologie, University of Münster, Wilhelm-Klemm-Straße 10, 48149 Münster, Germany
[b] Nuclear & Chemical Sciences Division, Lawrence Livermore National Laboratory, 7000 East Avenue (L-231), Livermore, CA 94550, USA
[c] Department of Earth, Environmental and Planetary Sciences, Case Western Reserve University, 10900 Euclid Avenue, Cleveland, OH 44106, USA

Received 1 February 2019; accepted in revised form 29 May 2019; available online 5 June 2019

Abstract

Fifteen H, L, and LL ordinary chondrites of petrologic types 4–6 have been analyzed for Hf-W isotope systematics to constrain the chronology, internal structure, and thermal history of their parent bodies. For most samples coarse-grained metals plot below the isochrons defined by silicate-dominated fractions which consist of variable mixtures of silicate minerals with tiny metal inclusions. This offset results from an earlier Hf-W closure in the large metal grains and provides a new means for simultaneously determining cooling rates and Hf-W closure ages for individual samples. For most type 5 and 6 samples, cooling rates and Hf-W ages are inversely correlated, indicating that these samples derive from concentrically zoned bodies in which more strongly metamorphosed samples derive from greater depth. These data, therefore, provide strong evidence for a common 'onion shell' structure for the H, L, and LL chondrite parent bodies. The cooling rates and Hf-W ages of some type 5 and 6 chondrites overlap, indicating that the Hf-W systematics provide a more robust measure of the thermal history and burial depth of a given sample than the simple petrographic distinction between types 5 and 6. Two type 6 samples deviate from the correlation between cooling rates and Hf-W ages and cooled much faster than expected for their Hf-W age. These samples likely were excavated by impacts that occurred during high-temperature metamorphism and prior to complete closure of the Hf-W system at ~10 Ma after CAI formation. As these impacts would have disturbed the asteroid's cooling history, these samples likely derive from different bodies than samples with undisturbed cooling histories, implying that ordinary chondrites derive from more than just three parent bodies. The Hf-W data reveal that metal-silicate fractionation among the H, L, and LL groups occurred between ~2 and ~2.7 Ma after CAI formation and, hence, was about coeval to chondrule formation. As both metal-silicate fractionation and chondrule formation occurred prior to chondrite parent body accretion, there should be no ordinary chondrite chondrules that are younger than ~2.7 Ma. Finally, ordinary chondrite precursors had lower Hf/W ratios than carbonaceous chondrites, suggesting that inner and outer solar system materials, respectively, were chemically distinct even for refractory elements.

Keywords: W isotopes; Thermal metamorphism; Closure temperature; Cooling rates; Metal-silicate fractionation; Onion shell

1. INTRODUCTION

The short-lived ^{182}Hf-^{182}W system is a versatile chronometer that is widely applied to date planetary differentiation. Because Hf is lithophile, whereas W is siderophile, the Hf-W system is particularly useful to date

* Corresponding author at: Institut für Planetologie, Westfälische Wilhelms-Universität Münster, Wilhelm-Klemm-Straße 10, 48149 Münster, Germany.
E-mail address: jan.hellmann@uni-muenster.de (J.L. Hellmann).

https://doi.org/10.1016/j.gca.2019.05.040
0016-7037/

metal-silicate fractionation such as planetary core formation (Jacobsen, 2005; Kleine et al., 2009; Kleine and Walker, 2017). Recent advances in analytical techniques have led to a substantial increase in the precision of W isotope measurements (Kruijer et al., 2012; Touboul and Walker, 2012; Willbold et al., 2011), which now allow the resolution of sub-million-year age differences for metal samples (Kruijer et al., 2014a). For instance, these methods have successfully been applied to date iron meteorites, indicating that there are small differences in the time of core formation in their parent bodies (Kruijer et al., 2014a, 2017). However, the full potential of the Hf-W system to date chondrites and constrain the accretion and thermal history of their parent bodies has yet to be realized. Here we show that a small difference in the Hf-W closure temperature between metal and silicates led to resolvable differences in ^{182}W compositions that can be used to determine high temperature cooling rates for individual ordinary chondrites. This, combined with the ability of the Hf-W system to provide precise cooling ages provides critical new insights into the thermal history and internal structure of chondrite parent bodies.

Ordinary chondrites are the largest class of meteorites and sample at least three different parent bodies, characterized by distinct metal-to-silicate ratios and defining the three subgroups H, L, and LL. Subsequent to parent body accretion, most ordinary chondrites were thermally overprinted and as a result exhibit a range of metamorphic conditions from petrologic type 3 (unequilibrated) to types 4–6 (equilibrated) (Dodd, 1969). Estimated peak metamorphic temperatures are ~700 °C for type 4 chondrites and ~900–950 °C for type 6 chondrites (*e.g.,* Dodd, 1981; Keil, 2000; Kleine et al., 2008; Slater-Reynolds and McSween, 2005), although it is debated whether type 4 and 6 chondrites had distinct peak metamorphic temperatures or merely different cooling histories (Kessel et al., 2007). Chronological studies of ordinary chondrites are numerous, but major uncertainties exist regarding the timescales of chondrule formation and chondrite parent body accretion, as well as regarding the thermal and impact histories of the parent bodies. For instance, internal ^{26}Al-^{26}Mg isochron ages for individual chondrules from primitive ordinary chondrites cluster at ~2–3 million years (Ma) after the formation of Ca,Al-rich inclusions (CAI), indicating a narrow time interval for chondrule formation (*e.g.,* Kita et al., 2000; Kita and Ushikubo, 2012; Pape et al., 2019; Rudraswami and Goswami, 2007; Villeneuve et al., 2009). However, Pb-Pb ages for individual chondrules from the same type of chondrites exhibit a much wider range of ages and suggest that chondrule formation occurred for an extended period of up to ~4 Ma (Bollard et al., 2017). Further, thermochronological studies suggest that ordinary chondrite parent body accretion occurred at ~2 Ma after CAI formation, followed by thermal metamorphism through internal heating by decay of ^{26}Al and subsequent cooling over tens of Ma (Blackburn et al., 2017; Göpel et al., 1994; Trieloff et al., 2003). These processes probably resulted in an 'onion shell' structure of the parent bodies, in which the most strongly metamorphosed type 6 chondrites are located near the center and are surrounded by successive shells of less-metamorphosed type 5, 4 and 3 materials (Blackburn et al., 2017; Göpel et al., 1994; Trieloff et al., 2003). However, metallographic cooling rate data show no correlation between cooling rate and petrologic type, and this has led to the suggestion that either an onion shell structure never existed or that it was subsequently modified by impact-driven mixing of material from different parts of the interior (Scott et al., 2014; Taylor et al., 1987). Moreover, rapid high-temperature cooling rates inferred for some type 6 chondrites are also inconsistent with the onion shell model and have been used to argue for complete impact disruption and reassembly of ordinary chondrite parent bodies during high-temperature metamorphism (Ganguly et al., 2016). In this case, an onion shell structure would have probably never developed. However, a recent Pb-Pb dating study on phosphates from equilibrated ordinary chondrites suggests that an onion shell structure existed initially, but that the parent bodies were disrupted later, at ~60 Ma after CAI formation (Blackburn et al., 2017). These examples highlight that overall there is neither consensus on the timing of chondrule formation and parent body accretion, nor on the parent bodies' internal structures and impact histories.

The Hf-W system is ideally suited to address these issues. Owing to its high closure temperature of ~750–850 °C (Cherniak and Van Orman, 2014; Kleine et al., 2008), which is higher than the closure temperatures of other chronometers typically used for dating ordinary chondrites (*e.g.,* $T_C \sim 450$ °C for the Pb-Pb system in phosphates; Cherniak et al., 1991), the Hf-W system is more resistant against resetting by later thermal events. As such it provides robust constraints on the high-temperature cooling history and internal structure of ordinary chondrite parent bodies (Kleine et al., 2008). Moreover, the Hf-W system can be used to date metal-silicate fractionation among the ordinary chondrite subgroups. As this event should have predated the accretion of the ordinary chondrite parent bodies, this would provide a measure of the latest possible time of chondrule formation that is independent of the ages determined for individual chondrules.

Here, high-precision Hf-W isotopic data for 15 equilibrated H, L, and LL chondrites of petrologic types 4 to 6 are reported. These data are used to quantify the thermal and impact history of ordinary chondrite parent bodies, to assess their internal structure, and to determine the timescale of metal-silicate fractionation among the ordinary chondrite subgroups.

2. SAMPLES AND ANALYTICAL METHODS

2.1. Samples and sample preparation

Four H chondrites, six L chondrites, and five LL chondrites were selected for this study. All but one of the H chondrites were previously investigated for Hf-W systematics (Kleine et al., 2008), facilitating direct comparison of the new data to previously obtained results. The other samples either are falls or are meteorites from Northwest Africa (NWA) for which terrestrial weathering is minor to absent (W0–W2). Further, for Barwell (L5) and Bruderheim (L6)

precise Pb-Pb phosphate ages are available (Blackburn et al., 2017; Göpel et al., 1994), making it possible to reconstruct the cooling histories of these particular samples. The selected NWA meteorites have not been classified in detail before, and so a detailed petrographic classification of these meteorites has been performed as part of the present study. On the basis of Fe content in olivines and pyroxenes, texture, and grain size of secondary feldspar grains, the NWA chondrites of this study are classified as follows: NWA 7545 (LL4); NWA 6629 (LL5); NWA 6935 (LL5); NWA 5755 (LL6); NWA 6630 (L5). Note, however, that due to their somewhat larger plagioclase grain sizes, both NWA 6629 and NWA 6935 seem to be intermediate between type 5 and type 6 (see supplement for details about the classification).

Fragments of each chondrite were cleaned with abrasive paper and by sonication in de-ionized H_2O and ethanol. The samples were gradually crushed in an agate mortar to grain sizes of < 250 μm, while coarse metal grains (>250 μm) were removed with a hand magnet. Metals from the < 250 μm fraction were also removed with a hand magnet, and were purified by grinding and sonication in ethanol. The coarse metal grains (>250 μm) were purified in the same manner, so that two distinct metal fractions (M) of different grain sizes (<250 μm; >250 μm) were obtained. For the remaining fractions, fines (<40 μm) were removed from the silicate portion using a nylon sieve and the remaining material (40–250 μm) was successively divided into three silicate-dominated fractions of different magnetic susceptibility using a hand magnet. Although all visible metal grains were removed from these fractions, they still contain variable amounts of tiny metal inclusions, resulting in different magnetic susceptibilities. The least magnetic fraction is denoted "non-magnetic" (NM), whereas the two slightly more magnetic fractions are denoted "weakly magnetic", where WM-1 is less magnetic than WM-2. After the magnetic separation, the WM and NM fractions were cleaned in an ultrasonic bath with de-ionized water and ethanol and then dried using an infrared lamp.

2.2. Chemical separation and isotope measurements

All chondrite fractions were dissolved in 60 ml Savillex vials at 110–120 °C on a hotplate using 16 ml HNO_3–HCl–HF (10:5:1) for metal fractions and 12 ml HF–HNO_3 (2:1) for silicate-dominated fractions. Because of the low W concentrations in the silicates, triple-distilled HF (<0.2 pg W/ml) was used throughout this study to ensure low W blanks. After digestion, the samples were evaporated to dryness, and following several dry downs, completely dissolved in 6 M HCl–0.06 M HF. From these solutions 2–3% (metal fractions) or 10% (silicate-dominated fractions) aliquots were taken for Hf and W concentration measurements by isotope dilution using a mixed ^{180}Hf-^{183}W tracer (Kleine et al., 2004; 2002). The separation of W and Hf from the spiked (Kleine et al., 2004) and unspiked aliquots (Kleine et al., 2012; Kruijer et al., 2014b) followed our established procedures. After each chromatography step, the W cuts from the metal samples were dried in concentrated $HClO_4$ at high temperature to reduce W loss associated with incomplete re-dissolution in the PFA beakers (e.g., Kruijer et al., 2012). For the silicate-dominated fractions, however, no $HClO_4$ was used in order to keep the W blanks sufficiently low. For these samples, the dry-downs were performed with added HNO_3-H_2O_2 at low temperatures (max. 80 °C) (Kleine et al., 2004). The total procedural blanks ranged from ~10 to ~40 pg (silicate-dominated fractions) and ~100 to ~260 pg (metal fractions) for the W isotope composition measurements. For all measurements, the W blanks are <1% of the total W amount in the samples and small blank corrections were necessary only for some of the NM fractions, which contained less than ~2 ng W (Tables 1–3). The total procedural blanks for the isotope dilution measurements were 1–5 pg W and 1–6 pg Hf and were negligible for all samples.

All isotope measurements were performed using a ThermoScientific Neptune *Plus* MC-ICP-MS at the Institut für Planetologie. Samples were introduced using a Cetac Aridus II desolvator and Savillex C-flow nebulizers at an uptake rate of 50 μl/min. Using Jet sampler and X skimmer cones total ion beam intensities of $\sim 1.5–2 \times 10^{-10}$ A were obtained for a ~30 ppb W solution. Each measurement consisted of 60 s baseline integrations (deflected beam), followed by 100–200 isotope ratio measurements of 4.2 s each. Isobaric Os interferences on ^{184}W and ^{186}W were monitored on mass ^{188}Os and were negligible for all samples. Instrumental mass bias was corrected relative to $^{186}W/^{184}W = 0.92767$ ('6/4') using the exponential law, and results are reported as ε-unit deviations (*i.e.,* 0.01%) relative to the mean value of the bracketing solution standard (prepared from a pure Alfa Aesar W metal; Kleine et al., 2004) which was measured at the same concentration as the samples.

The accuracy and reproducibility of the sample analyses were assessed through measurements of a terrestrial rock standard (BHVO-2) and a metal standard (NIST 129c) that were processed together with the silicate-dominated fractions and metal separates. The average ε^{182}W (6/4) obtained for single 200 cycle analyses of BHVO-2 (Table S4) yields $\varepsilon^{182}W = -0.03 \pm 0.13$ (2 s.d., n = 15). This is consistent with the precision of the BHVO-2 analyses (±10 ppm) found in earlier high-precision W isotope studies (Kruijer et al., 2014b). For metal separates, results are reported as the mean of pooled solution replicates (n = 4–7) with their corresponding 95% confidence intervals. Seven individual digestions of NIST 129c analyzed this way (*i.e.,* 5 × 200 cycles) yield an average ε^{182}W (6/4) of 0.03 ± 0.05 (2 s.d., n = 7; Table S4). For silicate samples measured at lower intensities or for a shorter duration (100 cycles), the external reproducibility was assessed by measuring solution standards over a range of W concentrations (2–30 ppb). The results of these analyses define a correlation between internal run precision (2 s.e.) and external reproducibility (2 s.d.) of these measurements (Fig. S1). We therefore used the slope of this correlation and the internal precision (2 s.e.) obtained for individual sample analyses to calculate the external uncertainty (2 s.d.) for these analyses. Finally, the uncertainty on ^{180}Hf/^{184}W ratios is typically <1% (2σ) for silicate samples and <10% (2σ) for metal

Table 1
Hf-W data for metal, weakly magnetic (WM) and non-magnetic (NM) fractions of H chondrites.

Sample		Grain size (μm)	Weight (mg)	Hf (ppb)	W (ppb)	$^{180}Hf/^{184}W$ (±2σ)	N	Cycles	$\varepsilon^{182}W$ (6/4) (±2σ)[a]
ID	Fraction								
Ste. Marguerite (H4)									
AV01	Metal	>250	273	4.68	869	0.0064 ± 0.0004	5	200	−3.23 ± 0.05
AV02	Metal	<250	503	4.53	856	0.0062 ± 0.0002	5	200	−3.29 ± 0.05
AN01	WM-2	40–250	283	183	46.2	4.671 ± 0.013	1	100	0.80 ± 0.31
AN02	WM-1	40–250	531	168	20.5	9.669 ± 0.035	1	100	5.39 ± 0.35
AN03	NM	40–250	506	180	11.8	17.94 ± 0.17	1	100	12.45 ± 0.44
AX01	WM-2	40–250	578	173	69.5	2.941 ± 0.013	1	200	−0.68 ± 0.10
AX02	WM-1	40–250	537	176	19.9	10.47 ± 0.09	1	100	5.79 ± 0.42
AX03	NM	40–250	571	198	11.1	21.14 ± 0.38	1	100	14.75 ± 0.68
ALH 84069 (H5)									
AD05	Metal	150–250	272	4.84	816	0.0070 ± 0.0002	4	200	−3.08 ± 0.06
AD06	Metal	>250	343	5.48	818	0.0079 ± 0.0002	5	200	−3.03 ± 0.05
AU09	WM-2	40–250	521	199	60.6	3.880 ± 0.010	1	200	−0.27 ± 0.10
AU08	WM-1	40–250	527	183	33.8	6.367 ± 0.019	1	100	1.35 ± 0.28
AU07	NM	40–250	432	192	23.5	9.665 ± 0.038	1	100	3.67 ± 0.34
Estacado (H6)									
AD09	Metal	150–250	352	2.48	879	0.0033 ± 0.0002	5	200	−2.91 ± 0.08
AD10	Metal	>250	341	3.70	891	0.0049 ± 0.0002	6	200	−2.88 ± 0.05
AU03	WM-2	40–250	534	210	90.0	2.748 ± 0.009	1	200	0.00 ± 0.10
AU02	WM-1	40–250	527	141	27.1	6.144 ± 0.073	1	100	1.56 ± 0.27
AU01	NM	40–250	610	169	14.1	14.12 ± 0.62	1	100	5.01 ± 0.42
Zhovtnevyi (H6)									
AC04	Metal	<250	206	7.41	912	0.0096 ± 0.0006	5	200	−3.05 ± 0.08
AC05	Metal	>250	222	4.25	880	0.0057 ± 0.0005	5	200	−3.05 ± 0.07
AU06	WM-2	40–250	463	209	48.1	5.118 ± 0.015	1	100	0.94 ± 0.10
AU05	WM-1	40–250	535	154	11.4	16.00 ± 0.20	1	100	7.35 ± 0.41
AU04	NM	40–250	546	154	3.51	51.67 ± 1.66	1	100	26.52 ± 0.82[b]

[a] Uncertainties for metal samples are 95% confidence intervals for solution replicates ($N = 4$–7) or the 2 s.d. of several quintuple measurements of the NIST129c metal standard of ±0.05 $\varepsilon^{182}W$, whichever is larger; Uncertainties for WM-2 fractions measured for 200 cycles represent the long term reproducibility of ±0.10 $\varepsilon^{182}W$ as determined for replicate measurements of terrestrial rock standards (Kruijer et al., 2014b); uncertainties for all other silicate-dominated fractions were determined from the relation between within-run 2 s.e. and 2 s.d. external reproducibility estimated by replicate measurements of the solution standard at different intensities (see text and Supplement for details).

[b] Blank corrected values.

Table 2
Hf-W data for metal, weekly magnetic (WM) and non-magnetic (NM) fractions of L chondrites.

Sample		Grain size (μm)	Weight (mg)	Hf (ppb)	W (ppb)	$^{180}Hf/^{184}W$ (±2σ)	N	Cycles	$\varepsilon^{182}W$ (6/4) (±2σ)[a]
ID	Fraction								
Saratov (L4)									
AE01	Metal	<250	425	15.1	635	0.0281 ± 0.0005	5	200	−3.23 ± 0.09
AE02	Metal	>250	451	7.76	694	0.0132 ± 0.0004	5	200	−3.26 ± 0.05
AK01	WM-2	<250	485	175	88.0	2.343 ± 0.006	1	200	−1.19 ± 0.10
AK02	WM-1	<250	472	171	45.1	4.480 ± 0.012	1	100	0.75 ± 0.22
AK03	NM	<250	486	161	35.1	5.432 ± 0.014	1	100	1.75 ± 0.27
Tennasilm (L4)									
AE03	Metal	<250	368	23.0	716	0.0379 ± 0.0005	5	200	−3.17 ± 0.09
AE04	Metal	>250	428	17.3	821	0.0249 ± 0.0026	5	200	−3.23 ± 0.07
AI01	WM-2	40–250	489	170	86.8	2.318 ± 0.007	1	150	−1.24 ± 0.10
AI02	WM-1	40–250	508	172	43.6	4.649 ± 0.012	1	100	0.82 ± 0.29
AI03	NM	40–250	515	149	30.3	5.808 ± 0.017	1	100	1.97 ± 0.32
NWA 6630 (L5)									
AO03	Metal	<250	197	9.20	836	0.0130 ± 0.0003	4	200	−3.00 ± 0.06
AO04	Metal	>250	552	35.4	722	0.0579 ± 0.0002	6	200	−2.98 ± 0.06
AP01	WM-2	40–250	499	173	75.2	2.718 ± 0.008	1	200	−0.93 ± 0.10
AP02	WM-1	40–250	526	174	43.7	4.695 ± 0.021	1	100	0.43 ± 0.30
AP03	NM	40–250	520	181	32.3	6.597 ± 0.019	1	100	1.87 ± 0.36
Barwell (L5)									
AV03	Metal	>250	524	5.66	1228	0.0054 ± 0.0001	6	200	−2.95 ± 0.05
AV04	Metal	<250	148	6.08	1409	0.0051 ± 0.0004	6	200	−2.88 ± 0.05
AX04	WM-2	40–250	571	179	64.0	3.295 ± 0.014	1	200	−0.33 ± 0.10
AX05	WM-1	40–250	508	163	13.4	14.39 ± 0.15	1	100	7.14 ± 0.45
AX06	NM	40–250	527	174	4.00	51.24 ± 1.66	1	100	30.27 ± 0.71[b]
Kunashak (L6)									
AE05	Metal	<250	191	24.5	1089	0.0265 ± 0.0004	5	200	−2.75 ± 0.05
AE06	Metal	>250	406	11.7	1212	0.0114 ± 0.0003	7	200	−2.79 ± 0.05
AK04	WM-2	40–250	489	140	50.3	3.292 ± 0.008	1	100	−0.91 ± 0.25
AK05	WM-1	40–250	477	163	11.8	16.35 ± 0.04	1	100	7.28 ± 0.46
AK06	NM	40–250	514	187	4.61	47.81 ± 0.16	1	100	25.54 ± 0.67[b]
Bruderheim (L6)									
AO01	Metal	<250	213	21.6	1340	0.0190 ± 0.0002	5	200	−2.64 ± 0.08
AO02	Metal	>250	514	7.08	1167	0.0072 ± 0.0001	5	200	−2.79 ± 0.07
AP04	WM-2	40–250	453	172	88.9	2.285 ± 0.006	1	200	−1.06 ± 0.10
AP05	WM-1	40–250	536	151	15.2	11.704 ± 0.053	1	100	4.03 ± 0.58
AP06	NM	40–250	514	182	3.96	54.07 ± 1.33	1	100	25.99 ± 0.97[b]

[a] Uncertainties for metal samples are 95% confidence intervals for solution replicates ($N = 4$–7) or the 2 s.d. of several quintuple measurements of the NIST129c metal standard of ±0.05 $\varepsilon^{182}W$, whichever is larger; Uncertainties for WM-2 fractions measured for 200 cycles represent the long term reproducibility of ±0.10 $\varepsilon^{182}W$ as determined for replicate measurements of terrestrial rock standards (Kruijer et al., 2014b); uncertainties for all other silicate-dominated fractions were determined from the relation between within-run 2 s.e. and 2 s.d. external reproducibility estimated by replicate measurements of the solution standard at different intensities (see text and Supplement for details).

[b] Blank corrected values.

Table 3
Hf-W data for metal, weekly magnetic (WM) and non-magnetic (NM) fractions of LL chondrites.

Sample		Grain size (μm)	Weight (mg)	Hf (ppb)	W (ppb)	$^{180}Hf/^{184}W$ (±2σ)	N	Cycles	$\varepsilon^{182}W$ (6/4) (±2σ)[a]
ID	Fraction								
NWA 7545 (LL4)									
AF01	Metal	>250	303	11.2	1411	0.0094 ± 0.0002	5	200	−3.12 ± 0.05
AF02	Metal	<250	219	23.6	1188	0.0235 ± 0.0003	5	200	−3.06 ± 0.05
AL01	WM-2	40–250	350	205	148	1.633 ± 0.009	1	200	−1.58 ± 0.10
AL02	WM-1	40–250	495	210	51.8	4.784 ± 0.014	1	100	1.10 ± 0.23
AL03	NM	40–250	491	170	27.3	7.344 ± 0.043	1	100	3.21 ± 0.32
NWA 6935 (LL5)									
AF03	Metal	>250	262	7.27	2965	0.0029 ± 0.0001	5	200	−2.39 ± 0.05
AF04	Metal	<250	144	28.0	2404	0.0137 ± 0.0002	5	200	−2.34 ± 0.06
AL04	WM-2	40–250	357	113	155	0.856 ± 0.002	1	200	−1.53 ± 0.10
AL05	WM-1	40–250	488	127	19.9	7.559 ± 0.045	1	100	1.49 ± 0.39
AL06	NM	40–250	541	190	5.68	39.46 ± 1.05	1	100	15.16 ± 0.62
NWA 6629 (LL5)									
AO07	Metal	<250	77.9	6.09	1969	0.0036 ± 0.0004	5	200	−2.58 ± 0.09
AO08	Metal	>250	508	11.3	1551	0.0086 ± 0.0001	5	200	−2.60 ± 0.07
AP07	WM-2	40–250	383	143	145	1.162 ± 0.003	1	200	−1.72 ± 0.10
AP08	WM-1	40–250	524	144	22.7	7.489 ± 0.020	1	100	1.80 ± 0.51
AP09	NM	40–250	526	161	11.2	16.91 ± 0.09	1	100	6.53 ± 0.54
Tuxtuac (LL5)									
AM02	Metal	<250	143	14.1	2260	0.0073 ± 0.0004	5	200	−2.73 ± 0.10
AM03	Metal	>250	187	3.92	2941	0.0016 ± 0.0002	5	200	−2.72 ± 0.06
AN04	WM-2	40–250	514	147	114	1.523 ± 0.004	1	100	−1.60 ± 0.16
AN05	WM-1	40–250	505	131	34.0	4.558 ± 0.016	1	100	0.37 ± 0.27
AN06	NM	40–250	514	150	19.7	8.943 ± 0.065	1	100	3.06 ± 0.39
NWA 5755 (LL6)									
AF05	Metal	>250	121	25.2	2975	0.0100 ± 0.0002	5	200	−2.52 ± 0.05
AF06	Metal	<250	133	42.5	2510	0.0200 ± 0.0003	5	200	−2.45 ± 0.05
AN07	WM-2	40–250	514	155	113	1.621 ± 0.005	1	100	−1.73 ± 0.19
AN08	WM-1	40–250	507	154	33.0	5.524 ± 0.040	1	100	0.29 ± 0.30
AN09	NM	40–250	519	151	25.4	7.004 ± 0.114	1	100	1.15 ± 0.31

[a] Uncertainties for metal samples are 95% confidence intervals for solution replicates ($N = 4$–7) or the 2 s.d. of several quintuple measurements of the NIST129c metal standard of ±0.05 $\varepsilon^{182}W$, whichever is larger; Uncertainties for WM-2 fractions measured for 200 cycles represent the long term reproducibility of ±0.10 $\varepsilon^{182}W$ as determined for replicate measurements of terrestrial rock standards (Kruijer et al., 2014b); uncertainties for all other silicate-dominated fractions were determined from the relation between within-run 2 s.e. and 2 s.d. external reproducibility estimated by replicate measurements of the solution standard at different intensities (see text and Supplement for details).

samples, and mainly derives from the uncertainty on the isotope measurement.

In this study, only $^{186}W/^{184}W$-normalized data were used to avoid normalizations involving ^{183}W. The latter can be biased by a small analytical artefact on ^{183}W, most likely resulting from the nuclear field shift effect (Cook and Schönbächler, 2016; Kruijer et al., 2012; Willbold et al., 2011). This effect is present in most of the samples analyzed in the present study, including both chondrites and terrestrial samples (Tables S4-6). Previous studies have shown that this ^{183}W effect can be minimized through high-temperature dry downs with $HClO_4$ after each chromatographic separation. However, this procedure may introduce larger W blanks and was therefore avoided in the present study, leading to overall larger ^{183}W deficits in the present compared to recent high-precision W isotope studies. However, after correction for the ^{183}W effect, no resolvable ^{183}W anomalies remain for the chondrite samples, and the $\varepsilon^{182}W$ (6/4) and $\varepsilon^{182}W$ (6/3) values for each sample agree to within ± 3 ppm (Tables S5 and S6).

3. RESULTS

The Hf-W data for the metal and silicate fractions of the investigated chondrites are reported in Tables 1–3. All metal separates are characterized by low $^{180}Hf/^{184}W$ ratios (<0.03), demonstrating that almost pure metal separates were obtained, and have the lowest $\varepsilon^{182}W$ observed for samples of this study. Metal samples of all investigated type 4 chondrites have similar $\varepsilon^{182}W$ values of around −3.2, whereas metal from type 5 and 6 chondrites display more radiogenic values, the highest of which are observed for LL5 and LL6 chondrites. Further, for a given sample there is no $\varepsilon^{182}W$ difference between the physically separated >250 μm and <250 μm metal fractions (Tables 1–3). This contrasts with results from a prior study, which reported $\varepsilon^{182}W$ difference between different metal fractions from two H5 chondrites (Archer et al., 2019). The silicate-dominated fractions (*i.e.,* WM-2, WM-1, NM) of all investigated chondrites display decreasing W concentrations with decreasing magnetic susceptibility, indicating that the varying W contents predominantly reflect different metal contents. In these fractions metal probably occurs as small inclusions in silicate grains that could not be removed using a hand magnet. The silicate-dominated fractions also exhibit variable Hf contents, most likely reflecting varying amounts of high-Ca pyroxene, the major host of Hf. As a result, the $^{180}Hf/^{184}W$ ratios vary among the silicate-dominated fractions, and for each sample increase in the order WM-2 < WM-1 < NM.

The silicate-dominated fractions exhibit variable $\varepsilon^{182}W$ compositions, which for each sample are linearly correlated with $^{180}Hf/^{184}W$. For several samples, however, the coarse-grained metals plot below these correlation lines (Figs. 1–3). This is the case for all but one of the investigated LL chondrites and also for two H chondrites (Estacado and Zhovtnevyi), and two of the investigated L chondrites (Barwell and Bruderheim). By contrast, for the other L chondrites, and also for one LL6 chondrite (NWA 5755) and two H chondrites (Ste. Marguerite and ALH 84069), the coarse-grained metals plot on the $\varepsilon^{182}W$ versus $^{180}Hf/^{184}W$ correlations defined by the silicate-dominated fractions.

4. HF-W THERMOCHRONOMETRY OF ORDINARY CHONDRITES

4.1. General ^{182}Hf-^{182}W systematics

Given that the variable W concentrations of the silicate-dominated fractions predominantly reflect different abundances of metal inclusions, the linear correlations of $\varepsilon^{182}W$ with $^{180}Hf/^{184}W$ observed for each sample could in principle represent mixing lines between W-rich metal and W-poor silicates. Such mixing lines may not have chronological significance. However, a plot of Hf versus W shows that at least three components are necessary to account for the variable Hf and W concentrations observed (Fig. S2). As such, the different $^{180}Hf/^{184}W$ ratios of the silicate-dominated fractions do not only reflect different contents of fine-grained metals but also of high-Ca pyroxene, the major host of Hf. The $\varepsilon^{182}W$ versus $^{180}Hf/^{184}W$ correlations are, therefore, not binary mixing lines, but are isochrons. The initial $^{182}Hf/^{180}Hf$ ratios obtained from the isochrons defined by the silicate-dominated fractions correspond to Hf-W ages of ~3–4 Ma for type 4, ~6–14 Ma for type 5, and ~9–12 Ma for type 6 chondrites (Fig. 4a) [calculated using an initial $^{182}Hf/^{180}Hf = (1.018 \pm 0.043) \times 10^{-4}$ for CAIs; Kruijer et al., 2014b]. With two exceptions these ages are in good agreement with Hf-W ages reported for H4-6 chondrites in prior studies (Archer et al., 2019; Kleine et al., 2008). For the H4 chondrite Ste. Marguerite a Hf-W age of 1.7 ± 0.7 Ma was reported in a prior study (Kleine et al., 2008), which is older than the 3.8 ± 0.6 Ma age obtained in the present study. This difference most likely reflects the much higher precision achieved for the ^{182}W measurement performed in the present study. For the H4 chondrite Avanhandava, Archer et al. (2019) reported an apparent Hf-W age of ~9 Ma after CAIs, overlapping with ages typically observed for type 5 and 6 chondrites. However, the analyzed silicate fractions of Avanhandava have extremely high W concentrations, exceeding those of bulk H chondrites. This observation and the fact that the initial $\varepsilon^{182}W$ of the apparent Avanhandava isochron precisely provides the terrestrial W isotopic composition (initial $\varepsilon^{182}W = 0.00 \pm 0.09$; Archer et al., 2019) suggest strongly that this sample is affected by contamination with terrestrial W. As such, the chronological interpretation of the Hf-W data for Avanhandava remains ambiguous. Typical Hf-W ages for type 4 chondrites therefore are ~3–4 Ma after CAI formation, whereas the ages for type 5 and 6 chondrites are distinctly younger and, based on currently available data, extend to ~14 Ma after CAIs. Importantly, the Hf-W ages of type 5 and 6 chondrites overlap (Fig. 4a), suggesting that in terms of their cooling history there is no sharp boundary between samples of these petrologic types. We will return to this issue in Section 4.3 below.

A key observation from the new Hf-W data is that for several of the ordinary chondrites metal plots below the isochrons defined by the silicate-dominated fractions.

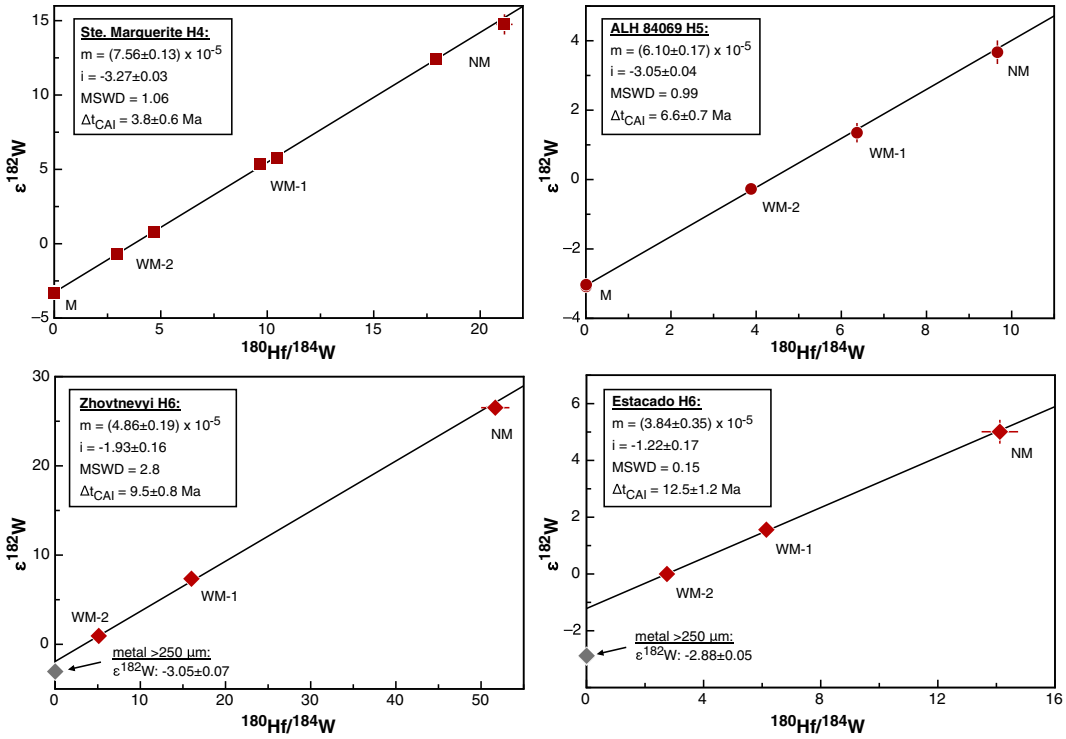

Fig. 1. $\varepsilon^{182}W$ vs. $^{180}Hf/^{184}W$ for H chondrites. m = initial $^{182}Hf/^{180}Hf$, i = initial $\varepsilon^{182}W$. Regressions calculated using model 1 fit of IsoPlot (Ludwig, 1991). Data shown as filled grey symbols (metal fractions) were not included in the regression. Δt_{CAI} is the formation interval relative to CAIs.

The latter contain various amounts of tiny metal grains, as is evident from their variable W contents, which correlate with the magnetic susceptibility of the different fractions (see above). The $\varepsilon^{182}W$ of these tiny metal grains is given by the intercept of the isochrons, and is elevated compared to the $\varepsilon^{182}W$ measured for the physically separated metal fractions. Thus, two distinct populations of metals having distinct ^{182}W compositions are present in most of the type 5 and 6 chondrites of this study. One population is represented by physically separated metal grains, whereas the other population is represented by tiny metal grains, which occur as inclusions in silicates and are characterized by more radiogenic $\varepsilon^{182}W$ compared to the large metal grains from the respective host chondrite. In a previous study, Archer et al. (2019) observed distinct $\varepsilon^{182}W$ values for >150 µm and <150 µm metal fractions from two H5 chondrites and suggested that this difference may reflect disequilibrium among individual metal grains in these samples. They also suggested that the offset of physically separated metals from the isochron defined by silicate fractions indicates a lack of metal-silicate equilibration in the ordinary chondrites. If this were true, then the ^{182}W composition of especially the metals would have limited chronological significance.

However, several lines of evidence indicate that the lower $\varepsilon^{182}W$ of the coarse-grained metal does not reflect the lack of isotopic equilibration with silicates, but instead results from slow subsolidus cooling. First, the $\varepsilon^{182}W$ values for type 5 and 6 metals (Fig. 4b) are more radiogenic than the composition expected for metal from primitive chondrites ($\varepsilon^{182}W \approx -3.3$), indicating that these metals isotopically equilibrated, at least in part, with radiogenic ^{182}W produced in the high-Hf/W silicates of their host chondrite. Second, metal-silicate disequilibrium should have resulted in variable $\varepsilon^{182}W$ of metal grains of distinct grain sizes, where the largest metal grains should have the lowest $\varepsilon^{182}W$. Although such distinct $\varepsilon^{182}W$ of metal grains have been observed by Archer et al. (2019) for two H5 chondrites, the ordinary chondrites of the present study display no $\varepsilon^{182}W$ differences between the <250 µm and >250 µm metal fractions; instead, only the tiny metal inclusions (≪40 µm) enclosed in the silicates have more elevated $\varepsilon^{182}W$. These ^{182}W systematics are an unlikely outcome of incomplete metal-silicate equilibration, which more likely would result in a range of ^{182}W compositions for metals of different grain sizes, and not in two distinct clusters of compositions. Finally, younger and hence more slowly cooled samples display a larger offset between the $\varepsilon^{182}W$ of physically separated metals and the initial $\varepsilon^{182}W$ of the isochron defined by the silicate-dominated fractions (Fig. 5). This correlation is opposite to what would be expected for metal-silicate disequilibrium, which should be more pronounced in less metamorphosed and faster cooled samples. By contrast, a larger $\varepsilon^{182}W$ difference between coarse-grained metal and the isochron initial for younger samples is expected for slow subsolidus cooling, where the W isotopic exchange between coarse-grained metals and surrounding silicates stopped before the Hf-W system closed in the silicate-dominated fractions. In this case, the time difference between Hf-W closure is larger

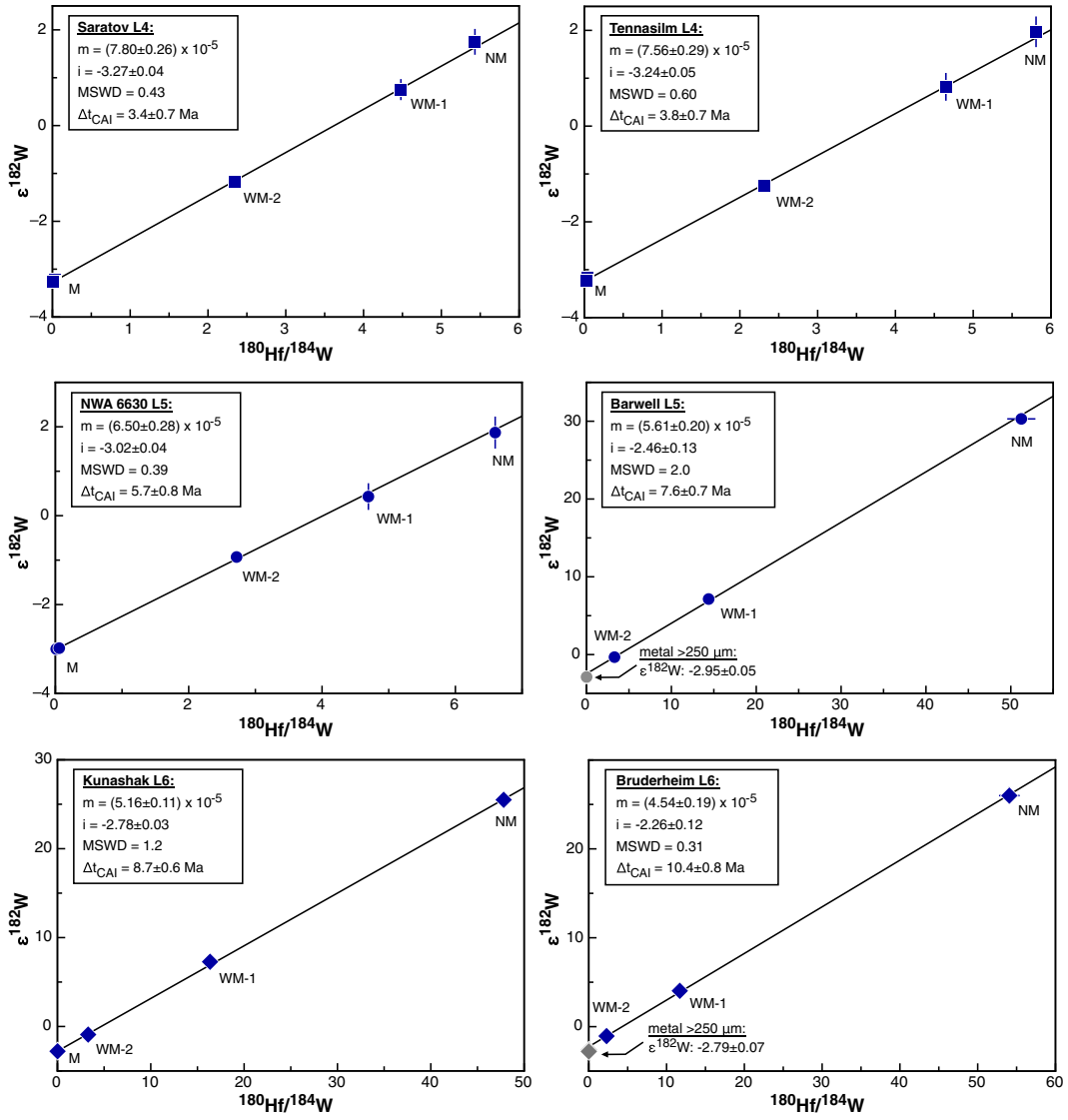

Fig. 2. $\varepsilon^{182}W$ vs. $^{180}Hf/^{184}W$ for L chondrites. m = initial $^{182}Hf/^{180}Hf$, i = initial $\varepsilon^{182}W$. Regressions calculated using model 1 fit of IsoPlot (Ludwig, 1991). Data shown as filled grey symbols (metal fractions) were not included in the regression. Δt_{CAI} is the formation interval relative to CAIs.

for samples that cooled more slowly, and so for these samples a larger $\varepsilon^{182}W$ difference between coarse-grained metals and the isochron intercept could evolve.

4.2. Distinct Hf-W closure temperatures for coarse- and fine-grained metal

Kleine et al. (2008) estimated values for the Hf-W closure temperature (T_C) in ordinary chondrites by numerical simulation of W diffusional exchange between high-Ca pyroxene (the major host of Hf and, hence, radiogenic ^{182}W) and metal (the sole sink for ^{182}W). The numerical model used by Kleine et al. (2008) to calculate closure temperatures was developed by Van Orman et al. (2006); it is similar to the "fast grain boundary" model developed by Eiler et al. (1992) for stable isotopes, extended to radioactive isotope systems by considering simultaneous radioactive production and decay. The model assumes that high-Ca pyroxene grains are always in contact with metal, either directly or via a network of grain boundaries through which diffusion is efficient enough to keep the surfaces of all mineral grains in equilibrium with each other. In cases where enough metal is present to provide an effectively infinite sink for radiogenic W, the following values for T_C were obtained: 800–875 °C (type 6); 750–850 °C (type 5); 725–850 °C (type 4).

These closure temperature estimates will change if (*i*) high-Ca pyroxenes are not in direct contact with metal, or (*ii*) the metal is not an effectively infinite sink. In the first case, T_C would be higher because the radiogenic ^{182}W would need to diffuse through orthopyroxene and olivine grains, and/or through a "slow" grain boundary network,

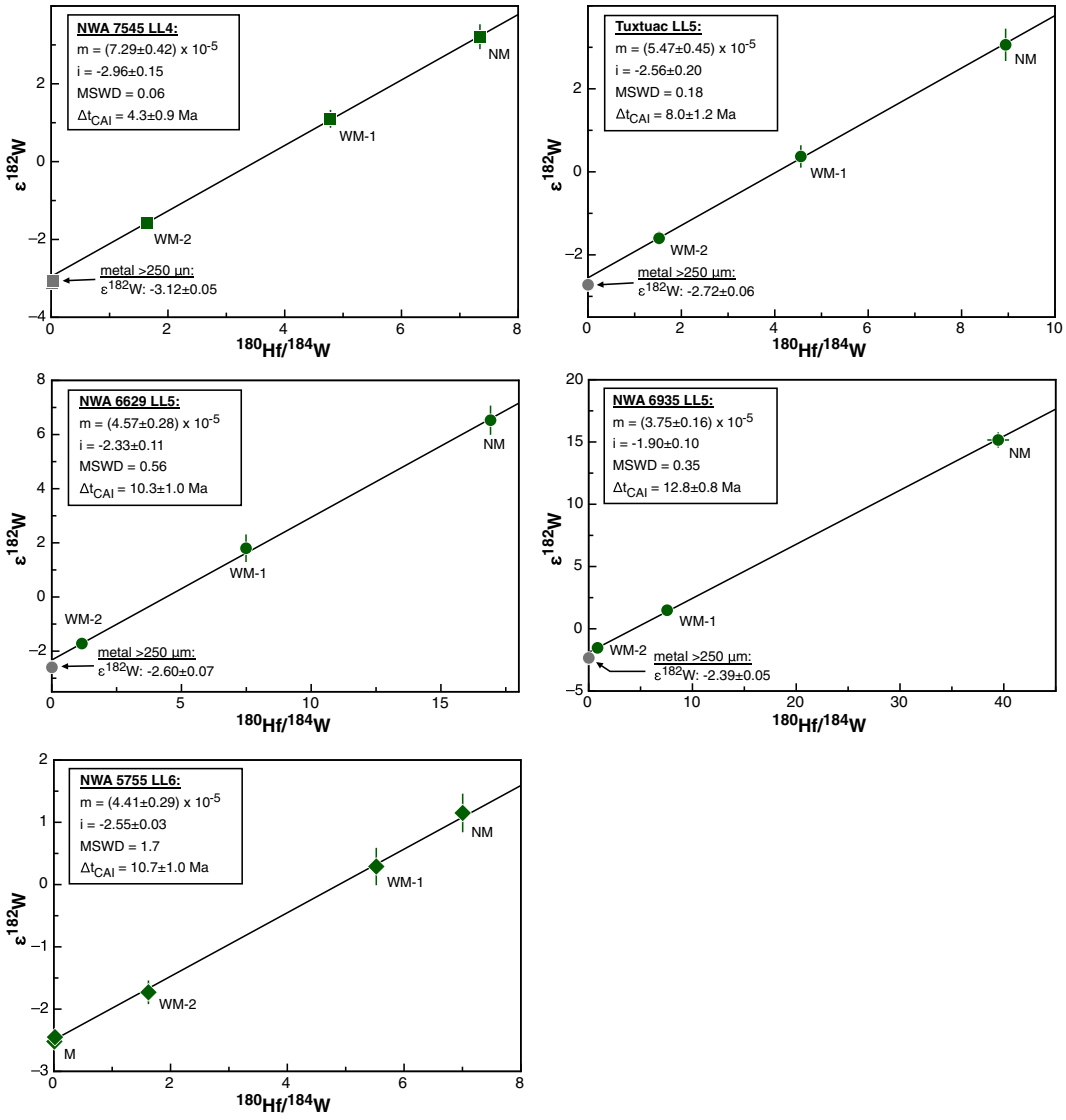

Fig. 3. $\varepsilon^{182}W$ vs. $^{180}Hf/^{184}W$ for LL chondrites. m = initial $^{182}Hf/^{180}Hf$, i = initial $\varepsilon^{182}W$. Regressions calculated using model 1 fit of IsoPlot (Ludwig, 1991). Data shown as filled grey symbols (metal fractions) were not included in the regression. Δt_{CAI} is the formation interval relative to CAIs.

before entering the metal (Cherniak and Van Orman, 2014; Kleine et al., 2008). Given the small grain size (5–30 μm in type 6 chondrites; Huss et al., 2006) and low abundance of high-Ca pyroxenes in ordinary chondrites, it seems likely that metal grains were often not in direct contact with these pyroxene grains, in which case T_C could be higher than the values given above. However, it is difficult to assess whether this effect could also be responsible for the distinct closure temperatures of coarse- and fine-grained metal. It is possible that for small metal grains interspersed between the silicate minerals there is a higher probability to be in direct contact with high-Ca pyroxenes, but the magnitude of this effect on T_C is difficult to determine and depends on several poorly constrained parameters, including the relative grain sizes of the silicate and metal grains, as well as the abundance and distribution of the fine-grained metals.

If the metal does not provide an effectively infinite sink, on the other hand, the closure temperature decreases. When the ratio of metal to high-Ca pyroxene becomes small, only a small amount of ^{182}W diffusing out of the silicates is sufficient to change the isotopic composition of the metal. In this case, the system remains open to significant radiogenic isotope exchange to lower temperatures than it would otherwise. Conversely, when the metal fraction is large it takes a larger diffusive flux of radiogenic ^{182}W to change the isotopic composition of the metal, and the closure temperature is therefore higher. Consequently, if the abundance of metal inclusions within the silicate-dominated fractions studied here is significantly smaller than the fraction of large metal grains in the bulk rock, the metal inclusions would be susceptible to W isotopic changes at lower temperatures than the large metal grains. This could poten-

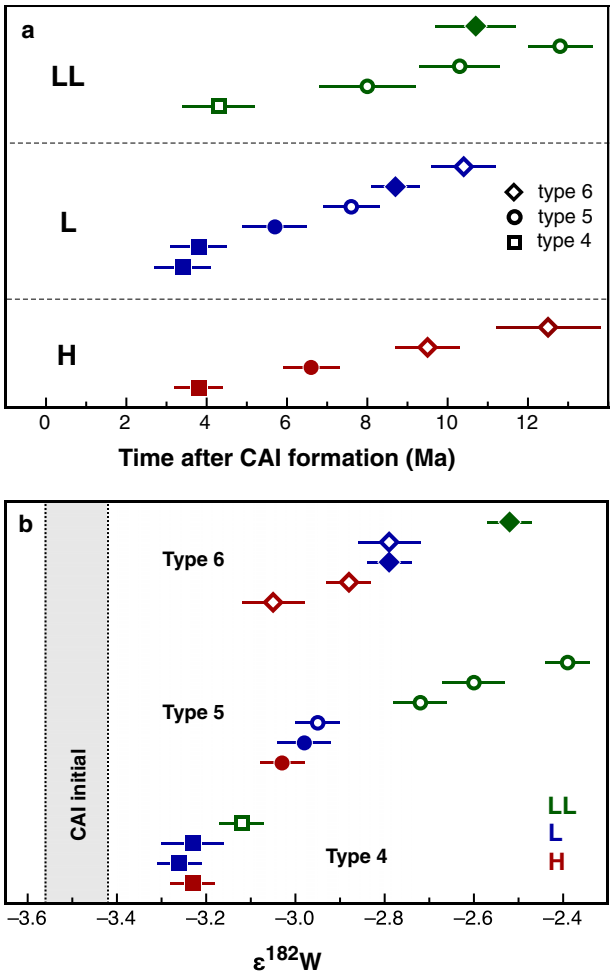

Fig. 4. (a) Hf-W isochron ages of ordinary chondrites. Solid symbols represent chondrites for which metal and silicates plot on single isochrons; open symbols represent samples for which metal plots below the isochron. For a given petrologic type, there are no systematic Hf-W age differences between H, L and LL chondrites, and in general, the ages become younger with increasing petrologic type. (b) Initial ε^{182}W of ordinary chondrites defined by their coarse-grained metals. Note that metals from all type 4 chondrites have similar ε^{182}W values. By contrast, metal from type 5 and 6 LL chondrites always has higher ε^{182}W compared to H and L metals of the same petrologic type (see Tables 1–3 for details).

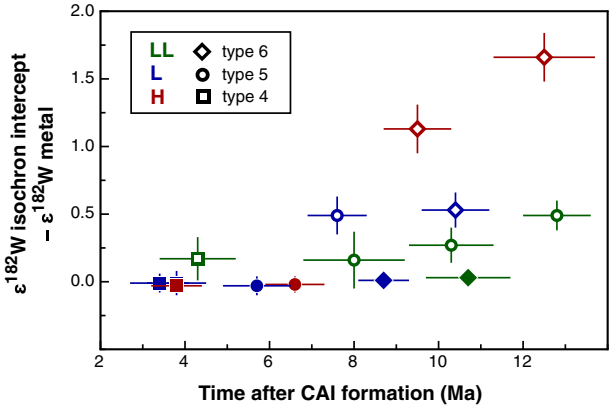

Fig. 5. Difference between the initial ε^{182}W of isochron defined by silicate-dominated fractions and ε^{182}W of coarse-grained metal versus Hf-W closure age for type 4, 5, and 6 chondrites. Closed symbols represent samples where metal and silicates plot on single isochrons; for samples shown with open symbols, coarse-grained metal and silicates do not plot on single isochrons. Generally, young samples display a larger offset in ε^{182}W between isochron intercept and coarse-grained metal than old samples, likely indicating slow subsolidus cooling.

tially explain the offset in ε^{182}W between the large metal grains and the silicate-dominated fractions.

To simulate how T_C changes as a function of the metal fraction, we have used the numerical model of Van Orman et al. (2006), which is the same model used by Kleine et al. (2008). In these simulations, ^{182}W is produced by radioactive decay within spherical grains of high-Ca pyroxene, and transferred to surrounding metal by diffusion through the high-Ca pyroxene as the system slowly cools. The temperature-dependent diffusion coefficient for W in high-Ca pyroxene was estimated using the model of Van Orman et al. (2001), as described in Kleine et al. (2008). All simulations assumed an initial temperature of 950 °C, a high-Ca pyroxene grain radius of 20 μm, and a cooling rate of 10 K/Ma. The silicate/metal partition coefficient for W, which determines the W concentration at the surfaces of the high-Ca pyroxene grains, was allowed to vary between 0.002 and 0.01. When the system has cooled to a temperature where diffusion is no longer significant, the simulation is stopped and the ε^{182}W compositions of the metal and high-Ca pyroxene (averaged over the spherical grains) are calculated. These record an apparent two-point isochron time, relative to the start of the simulation, and the closure temperature is the temperature that corresponds to this time. We simulated the closure temperature for systems with a wide range of metal fractions, with the results shown in Fig. 6.

To compare these modelling results to the actual Hf-W data, the metal fractions in the analysed bulk silicate-dominated fractions were estimated by mass balance as follows:

$$X_{metal} = \frac{[W]_{silicate-dominated} - D[W]_{metal}}{[W]_{metal} - D[W]_{metal}}$$

where $[W]_{\text{silicate-dominated}}$ is the weighted mean W concentration of all three silicate-dominated fractions (*i.e.,* the WM-2, WM-1 and NM fractions), $[W]_{\text{metal}}$ is the W concentration of the large metal grains, and D is the silicate-metal partition coefficient for W. For each sample, D was calculated by assuming that the NM fractions contain no metal and thus the measured W concentration of the NM fraction was used as the W concentration for silicates; if instead these fractions still contain some metal, D would be smaller and the calculated X_{metal} would be larger. However, for most samples the calculated D values are quite small (typically $\sim 4 \times 10^{-3}$), such that assuming even smaller values would not change the final X_{metal} significantly. For some samples (NWA 6630, Estacado, ALH 84069) the calculated D values are larger (~0.02–0.04), reflecting the higher W concentration in the NM fractions of these samples.

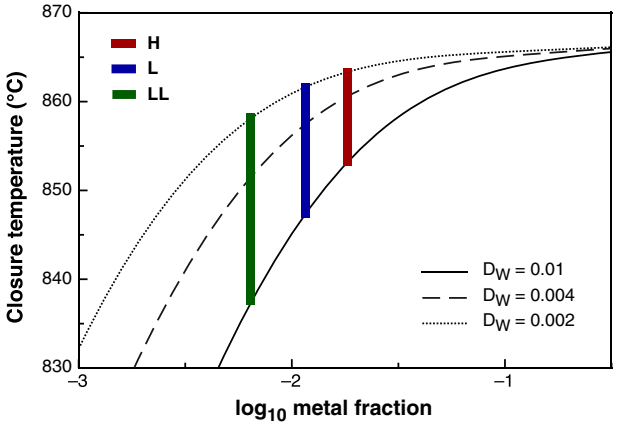

Fig. 6. Calculated closure temperatures for the Hf-W system as a function of metal fraction for different W silicate-metal partition coefficient (D_W). Calculations assume a peak temperature of 950 °C, a cooling rate of 10 °C/Ma and high-Ca pyroxene radius of 20 μm; these values are most appropriate for type 6 chondrites. Solid bars represent average metal fractions of the silicate-dominated fractions of type 5 and 6 chondrites (H, L, LL) (see Table S1 for details).

Although this could in principle reflect a larger metal fraction in the NM fractions, the same samples exhibit lower W concentrations in the metal (~850 ppb compared to ~1200 ppb in the other samples), consistent with a higher D value.

The metal fractions calculated for the bulk silicate-dominated fractions are fairly constant for samples from a given group but vary between the different groups: ~0.017 (H chondrites), ~0.012 (L chondrites) and ~0.006 (LL chondrites) (for details see supplement). These metal fractions are much lower than those estimated for the bulk chondrites, using the same equation and W concentrations for bulk H, L and LL chondrites of 190 ppb, 130 ppb and 90 ppb, respectively (Kleine et al., 2009): ~0.2 (H), ~0.1 (L) and ~0.03 (LL). Fig. 6 shows that these differences in metal fractions between the bulk silicate-dominated fractions and the bulk chondrites correspond to a difference in T_C of ~10–20 °C. As will be shown below, this difference in T_C, albeit quite small, is sufficient to result in resolvable offsets of coarse-grained metals from the isochrons.

4.3. Cooling rates of type 5 and 6 chondrites

The offset between the $\varepsilon^{182}W$ of coarse-grained metal and the initial $\varepsilon^{182}W$ of the isochron defined by the silicate-dominated fractions provides a new means for estimating cooling rates for type 5 and 6 chondrites. The time difference between Hf-W closure in the coarse-grained metals and the silicate-dominated fractions is given by:

$$\Delta t = \frac{1}{\lambda} \times \ln\left\{ \frac{\left(\frac{^{182}W}{^{184}W}\right)_{t_2} - \left(\frac{^{182}W}{^{184}W}\right)_{t_1}}{\left(\frac{^{180}Hf}{^{184}W}\right)_{silicate-dom.} \times \left(\frac{^{182}Hf}{^{180}Hf}\right)_{t_2}} + 1 \right\}$$

where t_1 is the time of metal closure and t_2 is the time of closure in the silicate-dominated fractions. The $^{182}W/^{184}W$ and $^{182}Hf/^{180}Hf$ at time t_2 are provided by the isochron of the silicate-dominated fractions, and the $^{182}W/^{184}W$ at time t_1 is that measured for the coarse-grained metals. The $^{180}Hf/^{184}W$ of the bulk silicate-dominated fraction (*i.e.,* all the material for which the Hf-W system is still open after closure of the coarse-grained metals) can be estimated from the weighted mean Hf and W concentrations measured for the silicate-dominated fractions (*i.e.,* WM-2, WM-1 and NM) for each sample. Thus, for each sample the time difference between Hf-W closure in coarse-grained metals and silicate-dominated fractions can be calculated. This information combined with the estimated difference in closure temperatures of 15 ± 5 °C (*i.e.,* the 10–20 °C estimate from above) then provides a cooling rate for each sample (Table 4 and Fig. 7).

The major source of uncertainty in the calculated cooling rates derives from uncertainties on the modeled closure temperature difference between coarse-grained metals and silicate-dominated fractions. As such it is useful to compare the calculated cooling rates to available thermochronological data for chondrites analyzed in the present study. This is possible for four of the investigated samples (Barwell, Bruderheim, Estacado, Tuxtuac), because for these samples Pb-Pb phosphate ages are available. Assuming undisturbed cooling between Hf-W and Pb-Pb closure and using Hf-W closure temperatures of 850 ± 50 °C (type 6) and 800 ± 50 °C (type 5), and a Pb-Pb closure temperature of 450 ± 50 °C, allows cooling rates to be calculated for each sample. The cooling rates calculated in this manner agree well with those deduced above from the ^{182}W difference between metal and the isochron intercept: Barwell (22 ± 8 °C/Ma from the Hf-W and Pb-Pb ages versus 22 ± 10 °C/Ma from the ^{182}W difference); Bruderheim (12 ± 4 versus 14 ± 6 °C/Ma); and Tuxtuac (30 ± 11 versus 28 ± 38 °C/Ma). Only for Estacado are the estimated cooling rates (9 ± 3 versus 2 ± 1 °C/Ma) different. This offset, as well as the very slow cooling inferred for Estacado, may indicate that the Hf-W system in Estacado does not record Hf-W closure during cooling from peak metamorphic temperatures but rather growth of high-Ca pyroxenes during prograde metamorphism (Kleine et al., 2008). Alternatively, Estacado may not have cooled undisturbed from Hf-W to Pb-Pb closure. For instance, Blackburn et al. (2017) argued that Pb-Pb phosphate ages for type 6 chondrites reflect impact disruption and subsequent rapid cooling. In this case the cooling of Estacado prior to disruption could have been slower than the calculated rate of 9 ± 3 °C/Ma, which assumes undisturbed cooling. In spite of these uncertainties, the good agreement between the cooling rates determined for the other samples suggests that the inferred closure temperature difference of 15 ± 5 °C between coarse-grained metals and silicate-dominated fractions is appropriate and can therefore be used to estimate accurate cooling rates.

Samples that show no resolvable ^{182}W difference between coarse-grained metal and the initial $\varepsilon^{182}W$ of the isochron may have cooled sufficiently fast so that no resolvable ^{182}W difference developed. Alternatively, these samples may lack the fine-grained metal interspersed in the silicate matrix. In this case the Hf-W system in the silicate and metal fractions of the entire sample would have closed

Table 4
Summary of the Hf-W systematics, cooling ages and cooling rates for type 5 and 6 ordinary chondrites. (a) Samples where metal plots below Hf-W isochron defined by silicate-dominated fractions; (b) samples where metal and silicate-dominated fractions define a single precise Hf-W isochron.

a	Metal > 250 μm	Hf-W isochron silicate-dominated fractions				Bulk silicate-dominated fraction	Metal closure		
Sample	$\varepsilon^{182}W$ (±95% conf.)	Initial $^{182}Hf/^{180}Hf$ ($\times10^{-5}$) (±2σ)	Initial $\varepsilon^{182}W$ (±2σ)	Δt_{CAI} (Ma) (±2σ)	$\Delta\varepsilon^{182}W_{isochron\ initial-metal}$ (±2σ) [a]	$^{180}Hf/^{184}W$	initial $^{182}Hf/^{180}Hf$ (x10^{-5}) (±2σ) [b]	$\Delta t_{metal-silicate}$ (Ma) (±2σ) [c]	Cooling rate (°C/Ma) (±2σ)
Estacado (H6)	−2.88 ± 0.05	3.84 ± 0.35	−1.22 ± 0.17	12.5 ± 1.2	1.66 ± 0.18	6.0	6.24 ± 0.44	6.2 ± 1.0	2 ± 1
Zhovtnevyi (H6)	−3.05 ± 0.07	4.86 ± 0.19	−1.93 ± 0.16	9.5 ± 0.8	1.13 ± 0.18	13.1	5.60 ± 0.22	1.8 ± 0.3	8 ± 3
Barwell (L5)	−2.95 ± 0.05	5.61 ± 0.20	−2.46 ± 0.13	7.6 ± 0.7	0.49 ± 0.14	13.7	5.92 ± 0.22	0.7 ± 0.2	22 ± 10
Bruderheim (L6)	−2.79 ± 0.07	4.54 ± 0.19	−2.26 ± 0.12	10.4 ± 0.8	0.53 ± 0.13	11.6	4.94 ± 0.21	1.1 ± 0.3	14 ± 6
NWA 6935 (LL5)	−2.39 ± 0.05	3.76 ± 0.16	−1.90 ± 0.10	12.8 ± 0.8	0.49 ± 0.11	10.0	4.18 ± 0.19	1.4 ± 0.4	11 ± 5
NWA 6629 (LL5)	−2.60 ± 0.07	4.57 ± 0.28	−2.33 ± 0.11	10.3 ± 1.0	0.27 ± 0.13	7.2	4.89 ± 0.32	0.9 ± 0.5	17 ± 11
Tuxtuac (LL5)	−2.72 ± 0.06	5.47 ± 0.45	−2.56 ± 0.20	8.0 ± 1.2	0.16 ± 0.21	5.9	5.71 ± 0.54	0.5 ± 0.7	28 ± 38

b	Metal >250 μm	Hf-W isochron bulk ordinary chondrite				Bulk silicate-dominated fraction	
Sample	$\varepsilon^{182}W$ (±95% conf.)	Initial $^{182}Hf/^{180}Hf$ ($\times10^{-5}$) (±2σ)	Initial $\varepsilon^{182}W$ (±2σ)	Δt_{CAI} (Ma) (±2σ)	$\Delta\varepsilon^{182}W_{isochron\ initial-metal}$ (±2σ) [a]	$^{180}Hf/^{184}W$	Cooling rate (°C/Ma)
ALH 84069 (H5)	−3.03 ± 0.05	6.10 ± 0.17	−3.05 ± 0.04	6.6 ± 0.7	−0.02 ± 0.06	5.6	>47
NWA 6630 (L5)	−2.98 ± 0.06	6.50 ± 0.28	−3.02 ± 0.04	5.7 ± 0.8	−0.04 ± 0.07	5.1	>46
Kunashak (L6)	−2.79 ± 0.05	5.17 ± 0.11	−2.78 ± 0.03	8.7 ± 0.6	0.01 ± 0.06	7.6	>54
NWA 5755 (LL6)	−2.52 ± 0.05	4.41 ± 0.29	−2.55 ± 0.03	10.7 ± 1.0	−0.03 ± 0.06	5.0	>30

[a] Measured difference in $\varepsilon^{182}W$ between metal and intercept of Hf-W isochron defined by silicate-dominated fractions.
[b] Calculated initial $^{180}Hf/^{182}Hf$ at the time of metal closure.
[c] Calculated difference in time between closure of metal and silicate-dominated fractions.

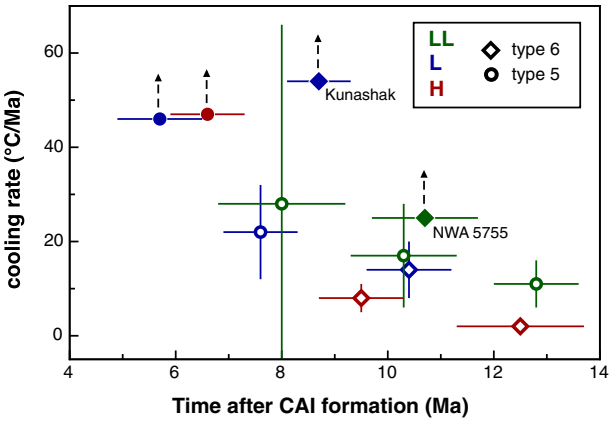

Fig. 7. Cooling rate versus Hf-W closure age for type 5 and 6 chondrites. The cooling rates were determined using the difference between the $\varepsilon^{182}W$ measured for coarse-grained metals and the intercept of the isochron defined by the silicate-dominated fractionations (see Table 4 and Eq. (2)) together with the difference in closure temperature. For samples shown with closed symbols metal and silicates plot on single isochrons, so that only minimum cooling rates can be determined. Most samples define an inverse correlation of cooling rates versus Hf-W ages, but two type 6 chondrites deviate from this trend. These samples were likely excavated to shallower depth during the high-temperature metamorphism.

simultaneously, because the large metal grains would have been the sole sink for radiogenic ^{182}W. A lack of fine-grained metal grains interspersed in the silicate matrix may result from oxidation of the metal, and would in this case lead to higher Fe contents of the surrounding olivine and orthopyroxene grains (Gastineau-Lyons et al., 2002). However, a plot of fayalite (Fa) versus ferrosilite (Fs) contents reveals no correlation between oxidation state and non-isochronous behavior of coarse-grained metals (Fig. S3, Table S2). This leaves rapid cooling as the most likely reason that in some samples the coarse-grained metals plot on the isochrons defined by the silicate-dominated fractions. Consequently, for these samples only minimum cooling rates can be estimated from the Hf-W data. Given a measurement precision of about ±0.05 for $\varepsilon^{182}W$ of the metals, an offset of as little as 0.1 $\varepsilon^{182}W$ between the coarse-grained metals and the initial $\varepsilon^{182}W$ of the silicate isochron would be resolvable. Using this difference in equation 2 provides the maximum time difference between Hf-W closure in the metals and the silicate-dominated fractions; if this time difference had been longer, then a > 0.1 $\varepsilon^{182}W$ difference between the metals and the isochron initial would have developed. Using this maximum time difference and the closure temperature difference of 15 ± 5 °C from above provides the following minimum cooling rates: >47 °C/Ma (ALH 84069), >46 °C/Ma (NWA 6630), >54 °C/Ma (Kunashak) and > 30 °C/Ma (NWA 5755) (Table 4).

4.4. Significance of Hf-W ages for type 4 chondrites

The apparent Hf-W ages for type 4 chondrites obtained in the present study are indistinguishable from each other and range from 3.4 ± 0.7 Ma for Saratov (L4) to 4.3 ± 0.9 Ma for NWA 7545 (LL4), post CAI formation. These ages are all younger than the ~2 Ma ^{26}Al-^{26}Mg ages for ordinary chondrite chondrules (*e.g.,* Kita et al., 2000; Kita and Ushikubo, 2012; Pape et al., 2019; Rudraswami and Goswami, 2007; Villeneuve et al., 2009), indicating that temperatures during thermal metamorphism were sufficiently high for at least some diffusional exchange of radiogenic ^{182}W. However, whether or not the Hf-W system was completely reset is unclear. As the Hf-W closure temperature for type 4 chondrites is similar to their peak metamorphic temperature (Kleine et al., 2008), the Hf-W system might have been only partially reset, in which case the apparent Hf-W age would predate the peak-metamorphic age. For instance, metallographic cooling rate data combined with a Pb-Pb phosphate age of Ste. Marguerite (4561.7 ± 0.7 Ma; Blackburn et al., 2017) have been interpreted to indicate impact excavation and rapid cooling at ~6 Ma after CAI formation. Thus, one possibility is that during this event the Hf-W system was incompletely reset, resulting in an apparent age that is intermediate between the original ~2 Ma and the ~6 Ma resetting age. However, the Hf-W ages of all type 4 chondrites investigated in this study are indistinguishable from each other, which seems an unlikely outcome of partial resetting during impact excavation. Nevertheless, it is noteworthy that coarse-grained metal from the LL4 chondrite NWA 7545 plots slightly below the isochron defined by the silicate-dominated fractions (Fig. 3). Although this difference is not clearly resolved, the MSWD of the isochron regression increases significantly when metal is included (MSWD = 1.7 if the metal is included versus 0.06 if the metal is excluded), suggesting that the metal does plot below the isochron. In principle, this could reflect slow cooling (the calculated cooling rate would be 37 ± 39 °C/Ma), but unlike for type 5 and 6 chondrites, it is unclear as to whether the Hf-W system in type 4 chondrites has been completely reset. Thus, it is also possible that in NWA 7545 equilibration was less complete for the coarse-grained metal compared to the fine-grained metal interspersed within the silicate matrix. In this case, the Hf-W data cannot be used to calculate cooling rates, highlighting that using the Hf-W system to determine cooling rates for type 4 chondrites is in general more difficult.

5. STRUCTURE AND THERMAL HISTORY OF ORDINARY CHONDRITE PARENT BODIES

5.1. A common onion shell structure for ordinary chondrite parent bodies

For almost all samples there is an inverse correlation of Hf-W ages and cooling rates as inferred from the offset between the $\varepsilon^{182}W$ of coarse-grained metals and the initial $\varepsilon^{182}W$ of the isochron defined by the silicate-dominated fractions (Fig. 7). Moreover, the youngest ages and lowest cooling rates are mostly observed for type 6 chondrites, whereas type 5 chondrites extend to older ages and faster cooling rates. Finally, for each ordinary chondrite group type 4 chondrites have the oldest ages (note that for these samples cooling rates cannot be inferred from the Hf-W data alone). All these observations indicate that more

strongly metamorphosed samples derive from greater depths, where cooling is slower and hence Hf-W closure occurred later. As such, these data provide strong support for the onion shell model for ordinary chondrite parent bodies. Until now, this model has mainly been considered for H chondrites (*e.g.,* Trieloff et al., 2003), but the data of this study demonstrate that it is also appropriate for the L and LL chondrite parent bodies. As samples from all three subgroups of ordinary chondrites (H, L, LL) define a similar range in ages (Fig. 4) and define a single correlation of cooling rates versus Hf-W ages (Fig. 7), their parent bodies likely had similar structures and high-temperature cooling histories and, hence, probably accreted at about the same time and had similar sizes.

In the specific sample set analyzed in this study, LL5 chondrites extend to younger ages than H5 and L5 samples, and also overlap with the Hf-W ages for H6 and L6 samples (Figs. 4 and 7). However, this likely reflects a sampling bias rather than a real difference in structure or thermal history of the LL compared to the L and H chondrite parent bodies. Moreover, the petrographic distinction between type 5 and 6 samples is not always straightforward and in fact there is no sharp boundary between these two types. Thus, there are samples that in terms of their thermal histories are transitional between type 5 and 6, and some of the older type 6 and younger type 5 chondrites may represent such samples. A corollary of this is that the correlation between cooling rates and Hf-W ages observed for most type 5 and 6 samples provides a more robust and distinctive measure of the burial depth of the samples and, hence, their metamorphic conditions and thermal history than the simple petrographic distinction between type 5 and 6. For instance, the two more quickly cooled type 5 chondrites investigated in this study (ALH 84069 and NWA 6630) must derive from a shallower depth than other type 5 samples, for which the inferred cooling rates are lower and the Hf-W ages are younger. Similarly, of the two H6 chondrites investigated, Estacado has a younger Hf-W age and slower cooling rate than Zhovtenvyi, indicating that it was located at a greater depth than the latter.

Based on the observation that metallographic cooling rates are not correlated with petrologic type, some prior studies have argued against cooling of ordinary chondrites in undisturbed onion shell structures (*e.g.,* Scott et al., 2014; Taylor et al., 1987). Further, Blackburn et al. (2017) observed that H6 and L6 chondrites have very consistent Pb-Pb phosphate ages and argued that this is unexpected for type 6 samples that cooled undisturbed at varying depths inside their parent bodies, because in this case a larger spread in ages would be expected. On this basis, Blackburn et al. (2017) inferred that the H and L chondrite parent bodies were catastrophically disrupted at ~60 Ma after CAI formation, leading to rapid cooling through Pb-Pb closure in phosphates. It is important to recognize, however, that the metallographic cooling rates and Pb-Pb phosphate ages record the cooling history at much lower temperatures (~400–500 °C) than the Hf-W system (~800–850 °C). Thus, any impact-induced mixing of material from different depths recorded in the metallographic cooling rates and Pb-Pb phosphate ages would not necessarily be recorded in the Hf-W systematics. For instance, at ~60 Ma (*i.e.,* the time of impact disruption inferred from Pb-Pb phosphate ages; Blackburn et al., 2017), the interior of the ordinary chondrite parent bodies had cooled well below the Hf-W closure temperature, meaning that the Hf-W system likely remained unaffected by this late event. Thus, the preservation of an initial onion shell structure in the Hf-W systematics of equilibrated ordinary chondrites is consistent with a later disturbance of this structure by impact disruption of these bodies, as seems to be required by the metallographic cooling rates and Pb-Pb phosphate ages.

5.2. Impact disruption and the number of ordinary chondrite parent bodies

Two type 6 chondrites (Kunashak and NWA 5755) plot above the correlation of cooling rates and Hf-W ages, and the minimum cooling rates for these samples at ~10 Ma are much faster than the expected cooling rates of ~10–20 °C/Ma for samples of this age (Fig. 7). The most obvious way to account for this more rapid cooling is impact excavation to shallower depths, where cooling is faster. Intriguingly, the $\varepsilon^{182}W$ of metal from Kunashak (L6) of -2.79 ± 0.05 is indistinguishable from that of the L6 chondrite Bruderheim ($\varepsilon^{182}W = -2.79 \pm 0.07$), suggesting that metal closure in these two samples occurred at about the same time, and that both samples were therefore initially located at similar depths. Thermal modelling indicates that type 6 chondrites with cooling rates of ~10 °C/Ma (*e.g.,* Bruderheim) are typically located at depth of several tens of km (*e.g.,* Henke et al., 2012; Taylor et al., 1987). Thus, the coeval Hf-W closure in Bruderheim and Kunashak metals together with the subsequent rapid cooling of Kunashak implies that this sample has been excavated from deep inside its parent body. Importantly, this impact excavation must have occurred prior to Hf-W closure in Kunashak at ~9 Ma, because otherwise metal and silicates would not plot on a single isochron. For NWA 5755 the situation is less clear, because this sample still plots close to the trend of cooling rate versus Hf-W age (Fig. 7). Note, however, that the cooling rate for this sample is a strict minimum cooling rate, meaning that its true cooling rate was likely higher, in which case NWA 5755 would also plot well above the correlation of cooling rate versus Hf-W age. This sample therefore was likely also excavated by impacts prior to cooling below Hf-W closure. The Hf-W evidence for early impact excavation is consistent with results of a diffusion modeling study, in which extremely rapid cooling rates inferred for some type 5 and 6 chondrites were attributed to impact disruption events at ~10 Ma after CAI formation (Ganguly et al., 2016).

Taken together, the Hf-W data indicate that at about 10 Ma after CAI formation some ordinary chondrite parent bodies were affected by impacts of sufficient size and energy to excavate material from their deep interiors. These impacts occurred early, during the high-temperature metamorphism and before cooling of other type 6 material below Hf-W closure. This is in contrast with the Hf-W evidence for undisturbed cooling in concentrically layered

bodies preserved in most of the investigated ordinary chondrites, indicating that their parent bodies remained largely intact during the period of high-temperature metamorphism. Although it may be possible that the conditions during impact excavation were such that they did not disturb the high-temperature cooling history of large parts of the parent body, it seems more likely that type 6 samples with distinct cooling histories derive from separate parent bodies. In this case, samples from each subgroup of ordinary chondrites (H, L, LL) would derive from multiple parent bodies, where some of these bodies remained intact, whereas other bodies were catastrophically disrupted by impacts and re-accreted. Of note, ordinary chondrites are by far the most common meteorite type, rendering it quite likely that they derive from more than just three parent bodies. Consistent with this, recent work has shown that H chondrites have distinct nucleosynthetic Mo isotope compositions, requiring at least two different H chondrite parent bodies (Worsham et al., 2017).

6. METAL-SILICATE FRACTIONATION AMONG CHONDRITE GROUPS

6.1. Timing of Hf-W fractionation and chondrule formation

The ordinary chondrite groups (H, L, LL) are characterized by distinct metal-to-silicate ratios and should therefore also be characterized by distinct Hf/W ratios. The data of the present study can be used to test this idea and, ultimately, to date the metal-silicate fractionation among the ordinary chondrite groups using the Hf-W system. In a diagram of initial $\varepsilon^{182}W$ versus initial $^{182}Hf/^{180}Hf$, samples formed at different times from a reservoir with a common $^{180}Hf/^{184}W$ plot along a straight line, whose slope corresponds to the $^{180}Hf/^{184}W$ ratio of the host reservoir. Thus, samples from a given ordinary chondrite group should plot on a single Hf-W isotope evolution line, and the different groups should define distinct lines according to their variable $^{180}Hf/^{184}W$ ratios. However, for samples for which coarse-grained metal and silicates do not plot on single isochrons (*i.e.,* for most of the type 5 and 6 samples of this study), the Hf-W evolution of bulk ordinary chondrites cannot be deduced using the initial $\varepsilon^{182}W$ and $^{182}Hf/^{180}Hf$ obtained from the isochron regressions. For these samples, the $\varepsilon^{182}W$ measured for the coarse-grained metal and the $^{182}Hf/^{180}Hf$ inferred for the time of metal closure must be used instead (Table 4). As shown in Fig. 8, the ordinary chondrites of this study plot on three distinct evolution lines, where each line is defined by samples from a given group (*i.e.,* H, L, or LL). The only sample that does not plot on the correlation line of its host group is Estacado. The reason for this offset is unclear at present but most likely is related to the fact that for this sample the $\varepsilon^{182}W$ difference between coarse-grained metal and isochron intercept is quite large. As such, the inferred time of metal closure in this sample is more uncertain and is strongly dependent on the $^{180}Hf/^{184}W$ of the bulk silicate-dominated fraction inferred for this sample. For instance, if this ratio is higher than estimated from the data of this study, then the inferred time of metal closure would be later and Estacado may then plot on the evolution line defined by the other H chondrites. There is no obvious reason for why the $^{180}Hf/^{184}W$ of Estacado's bulk silicate-dominated fraction should be different from the estimated ratio, but in principle this could result from sample heterogeneity and hence unrepresentative sampling through the particular piece analyzed. Regardless, Estacado is the only sample for which these inconsistencies exist, and for all other samples consistent Hf-W isotopic evolution lines are obtained.

The $^{180}Hf/^{184}W$ ratios derived from the slopes of the isotopic evolution lines are 1.17 ± 0.28 (H), 1.59 ± 0.19 (L) and 1.68 ± 0.20 (LL) ($\pm 2\sigma$). These ratios increase with decreasing metal-to-silicate ratios of the ordinary chondrites, indicating that the Hf-W fractionation most likely results from metal-silicate fractionation among the ordinary chondrite groups. The timing of this metal-silicate fractionation can thus be determined through the $^{182}Hf/^{180}Hf$ ratio at which the evolution lines intersect each other. Fig. 8 reveals that all three evolution lines intersect for $^{182}Hf/^{180}Hf$ ratios larger than $\sim 8.2 \times 10^{-5}$, which corresponds to an age of <2.7 Ma after CAI formation and therefore indicates that the Hf-W fractionation must have occurred prior to that time. As the evolution lines overlap within their uncertainties for $^{182}Hf/^{180}Hf$ ratios larger than $\sim 8.2 \times 10^{-5}$, the time of metal-silicate fractionation cannot be determined more precisely in this manner. However, the earliest possible time of metal-silicate fractionation can be constrained from the back projection of the evolution lines to the initial $\varepsilon^{182}W$ of CAIs. As CAIs are thought to be the first solids formed in the solar system, there should be no $\varepsilon^{182}W$ smaller than the initial value of CAIs. Of the three evolution lines, the L chondrite evolution line progresses to the lowest $\varepsilon^{182}W$ and, consequently, provides the tightest constraints on the earliest possible time of Hf-W fractionation (Fig. 8b). Back-projection of the L chondrite evolution line reveals that it would pass through the initial $\varepsilon^{182}W$ of CAIs at 1.6 ± 0.9 Ma after CAI formation, meaning that the Hf-W fractionation among the ordinary chondrite subgroups was established later than this time. Note that this is a strict minimum estimate, as this age is derived from the unrealistic assumption of $^{180}Hf/^{184}W = 0$ for the L chondrite precursors.

The difference between the $\varepsilon^{182}W$ of the L chondrite reservoir at the time of metal-silicate fractionation and the initial $\varepsilon^{182}W$ of CAIs can be used to calculate the $^{180}Hf/^{184}W$ ratio of the ordinary chondrite precursor reservoir prior to metal-silicate fractionation. Fig. 9 illustrates that for a metal-silicate fractionation prior to 2 Ma after CAI formation, the precursor's $^{180}Hf/^{184}W$ would be smaller than ~ 0.7. Such low $^{180}Hf/^{184}W$ ratios have so far only been measured for EH chondrites (Lee and Halliday, 2000), but other chondrites, including ordinary chondrites, all have higher $^{180}Hf/^{184}W$. As such it seems unlikely that the ordinary chondrite precursors had $^{180}Hf/^{184}W$ ratios much smaller than ~ 0.7, implying that the metal-silicate fractionation among ordinary chondrites cannot have occurred earlier than ~ 2 Ma after CAI formation (Fig. 9). This, combined with the upper limit of 2.7 Ma deduced above, reveals that the metal-silicate fractionation was coeval to chondrule formation at ~ 2–3 Ma after CAIs as dated

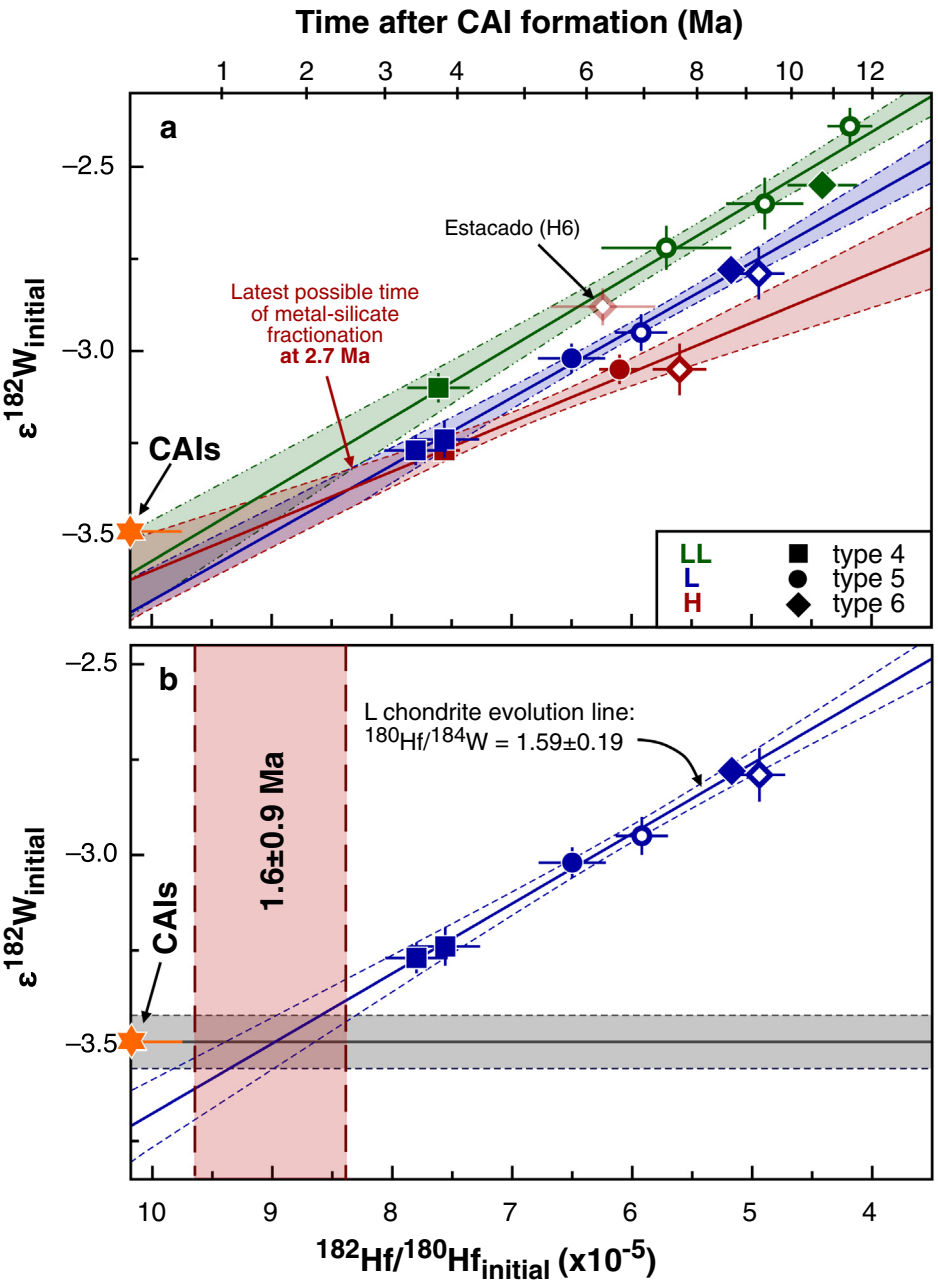

Fig. 8. (a) Initial $\varepsilon^{182}W$ and $^{182}Hf/^{180}Hf$ for ordinary chondrites from this study. For samples shown with closed symbols, metals and silicates define single isochrons. For samples shown with open symbols, coarse-grained metal and silicates do not plot on single isochrons; for these samples the Hf-W evolution of bulk ordinary chondrites cannot be deduced using the initial $\varepsilon^{182}W$ and $^{182}Hf/^{180}Hf$ obtained from the isochron regressions, but the $\varepsilon^{182}W$ measured for the coarse-grained metal and the $^{182}Hf/^{180}Hf$ inferred for the time of metal closure must be used instead. The H, L, and LL chondrites define three different evolution lines, consistent with distinct $^{180}Hf/^{184}W$ of their host reservoirs. The only sample that does not plot on the evolution line of its host group is Estacado (see text for details). The evolution lines overlap for $^{182}Hf/^{180}Hf > 8.2 \times 10^{-5}$, indicating that the distinct $^{180}Hf/^{184}W$ ratios of the H, L, and LL chondrites were established before 2.7 Ma after CAI formation. (b) Only the L chondrite evolution line is shown. The grey solid line represents the evolution of a primitive reservoir with $^{180}Hf/^{184}W = 0$, starting from CAIs. The intersection of both lines provides a lower limit for metal-silicate fractionation at 1.6 ± 0.9 Ma after CAIs (this uncertainty includes the uncertainty on the initial $\varepsilon^{182}W$ of CAIs and therefore is inconsistent with the red box plotted in the figure; in the figure the uncertainty on the CAI initial is shown separately).

by ^{26}Al-^{26}Mg chronometry (*e.g.,* Kita et al., 2000; Kita and Ushikubo, 2012; Pape et al., 2019; Rudraswami and Goswami, 2007; Villeneuve et al., 2009). This temporal overlap between chondrule formation and metal-silicate fractionation implies a causal link between these two processes, such as aerodynamic sorting of chondrules and metal grains (Jacquet, 2014). Finally, the latest possible time of metal-silicate fractionation of ~2.7 Ma after CAI forma-

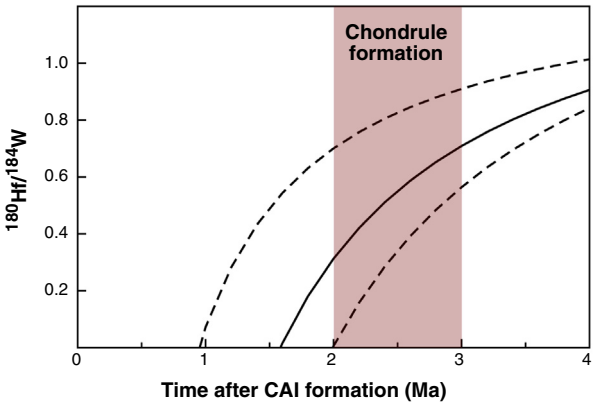

Fig. 9. $^{180}Hf/^{184}W$ of the ordinary chondrite precursor versus time of metal-silicate fractionation. A later time of metal-silicate fractionation implies a higher $^{180}Hf/^{184}W$ in the precursor. The $^{180}Hf/^{184}W$ ratios are calculated from the difference between the initial $\varepsilon^{182}W$ of CAIs and the back projected initial $\varepsilon^{182}W$ of the L chondrites, using their $^{180}Hf/^{184}W = 1.59 \pm 0.19$. Solid lines show results for $^{180}Hf/^{184}W = 1.59$, and dashed lines indicate the uncertainties resulting from uncertainties in this ratio. Shaded area denotes the time of chondrule formation (see text for details).

tion also implies that there should be no younger chondrules in ordinary chondrites. This is because it is difficult to envision any reasonable process of metal-silicate fractionation that would postdate parent body accretion and chondrule formation. As such, Pb-Pb ages of > 3 Ma reported for some ordinary chondrite chondrules (Bollard et al., 2017) probably do not provide the time of chondrule formation.

6.2. Distinct Hf/W ratios for the non-carbonaceous and carbonaceous meteorite reservoirs

Compared to the ordinary chondrite precursors, carbonaceous chondrites evolved with a higher $^{180}Hf/^{184}W$ of 1.37 ± 0.11, as inferred from linear regression of the initial $\varepsilon^{182}W$ and $^{182}Hf/^{180}Hf$ of CAIs, CV and CR chondrites, as well as the present-day $\varepsilon^{182}W$ of bulk carbonaceous chondrites (Budde et al., 2016, 2018; Kruijer et al., 2014b). This ratio is higher than the $^{180}Hf/^{184}W$ ratio inferred for the precursor material of ordinary chondrites (Fig. 9), most likely reflecting distinct metal-to-silicate ratios for the carbonaceous and non-carbonaceous meteorite reservoirs. This would be consistent with derivation of these meteorites from distinct regions of the solar protoplanetary disk that evolved independently of each other and presumably were separated by Jupiter (Budde et al., 2016; Kruijer et al., 2017; Warren, 2011).

Kruijer et al. (2017) demonstrated that the $\varepsilon^{182}W$ values of carbonaceous iron meteorites are systematically higher than those of non-carbonaceous irons (Kruijer et al., 2014a). This difference may reflect a slightly later time of core formation in the carbonaceous iron parent bodies. However, the results of this study reveal that this difference may also reflect distinct Hf/W ratios of their parent bodies. For instance, assuming that prior to differentiation the parent bodies of non-carbonaceous irons were characterized by $^{180}Hf/^{184}W \approx 0.7$ (the value inferred above for ordinary chondrite precursors) results in Hf-W model ages of $\sim$2 Ma after CAI formation, consistent with the core formation ages determined for the parent bodies of carbonaceous iron meteorites using the $^{180}Hf/^{184}W$ of carbonaceous chondrites (Kruijer et al., 2017).

7. CONCLUSIONS

This study comprises the largest set of Hf-W ages for equilibrated ordinary chondrites to date, and is the first study to provide precise Hf-W ages for L and LL chondrites. The Hf-W ages of H, L, and LL ordinary chondrites of petrologic types 4–6 range from $\sim$3–4 Ma for type 4 up to $\sim$14 Ma after CAI formation for some type 5 and 6 chondrites. Whereas the Hf-W ages of the type 5 and 6 chondrites date the timing of cooling from peak metamorphic temperatures below the Hf-W closure temperature, the chronological significance of the Hf-W ages for type 4 chondrites is less clear, because the Hf-W system in these chondrites might have been only partially reset. For most type 5 and 6 chondrites, physically separated metals plot below the isochron defined by silicate-dominated fractions, which consist of silicate minerals with varying amounts of tiny metal inclusions. The offset of the large metal grains from the isochrons results from a small difference in the effective Hf-W closure temperature, which is slightly higher in the large metal grains compared to the tiny metal inclusions in the silicate minerals. This offset provides a new means for simultaneously determining cooling rates and Hf-W closure ages for individual samples. For most type 5 and 6 samples, cooling rates and Hf-W ages are inversely correlated, indicating that these samples derive from concentrically zoned bodies in which more strongly metamorphosed samples derive from greater depth. These data, therefore, provide strong evidence for a common 'onion shell' structure for the H, L, and LL chondrite parent bodies. Moreover, the cooling rates and Hf-W ages of some type 5 and 6 chondrites overlap, and some type 5 samples have younger Hf-W ages and slower cooling rates compared to some type 6 samples. These observations indicate that the Hf-W systematics provide a more robust measure of the thermal history and burial depth of a given sample than the simple petrographic distinction between types 5 and 6.

For two type 5 and two type 6 samples, large metal grains plot on the isochron defined by the silicate-dominated fractions, indicating that these samples cooled sufficiently fast so that no resolvable ^{182}W difference between large metal grains and small metal inclusion developed. The two type 5 samples have the oldest Hf-W ages among the type 5 and 6 samples analyzed in this study, and they plot on the extension of the inverse correlation between cooling rates and Hf-W ages defined by the other samples. As such, these two type 5 samples likely derive from a shallower depth than the other samples, where cooling was faster. By contrast, the two type 6 samples for which the coarse-grained metals plot on the isochron defined by the silicate-dominated fractions plot off the cooling rate versus Hf-W age correlation and cooled much

faster than expected for their Hf-W age. These samples likely were excavated by impacts that occurred during high-temperature metamorphism and prior to complete closure of the Hf-W system at ~10 Ma after CAI formation. As these impacts would have disturbed the asteroid's cooling history, these samples likely derive from different bodies than samples with undisturbed cooling histories, implying that ordinary chondrites derive from more than just three (*i.e.,* H, L, LL) parent bodies.

The internal Hf-W isotope systematics demonstrate that the H, L, and LL chondrites evolved with distinct Hf/W ratios, which were established during metal-silicate fractionation among the ordinary chondrite groups. The Hf-W data reveal that this metal-silicate fractionation was about coeval with chondrule formation at ~2–3 Ma after CAI formation, indicating a causal link between these processes such as, for instance, aerodynamic sorting of chondrules and metal grains. Finally, the Hf/W ratio of the ordinary chondrite precursors were lower than those of carbonaceous chondrites, consistent with the idea that these two types of materials derive from distinct areas of the solar protoplanetary disk, which presumably were separated by Jupiter.

ACKNOWLEDGEMENTS

Some of the meteorite samples for this study were provided by the Natural History Museum, United Kingdom in London (Barwell; BM1985,M68), the Muséum national d'Histoire naturelle, France in Paris (Ste. Marguerite; MNHN 3290 and MNHN 2391), and NASA (ALH 84069). These sources of the meteorite specimens are gratefully acknowledged. This paper benefited greatly from discussions with Terrence Blackburn, which led us to focus the paper in a more significant direction. We thank Terrence Blackburn, Liping Qin, an anonymous reviewer, and associate editor Sara Russell for their thorough and constructive reviews. Some of this work was conducted under the auspices of the US Department of Energy at Lawrence Livermore National Laboratory, United States under Contract DE-AC52-07NA27344 (Release number: LLNL-JRNL-748444). This work was partially supported by funds from the Deutsche Forschungsgemeinschaft, Germany (SFB-TRR 170) and NASA, United States (NNX13AF58G). These sources of funding are gratefully acknowledged.

APPENDIX A. SUPPLEMENTARY MATERIAL

Supplementary data to this article can be found online at https://doi.org/10.1016/j.gca.2019.05.040.

REFERENCES

Archer G. J., Walker R. J., Tino J., Blackburn T., Kruijer T. S. and Hellmann J. L. (2019) Siderophile element constraints on the thermal history of the H chondrite parent body. *Geochim. Cosmochim. Acta* **245**, 556–576.

Blackburn T., Alexander C. M. O. D., Carlson R. and Elkins-Tanton L. T. (2017) The accretion and impact history of the ordinary chondrite parent bodies. *Geochim. Cosmochim. Acta* **200**, 201–217.

Bollard J., Connelly J. N., Whitehouse M. J., Pringle E. A., Bonal L., Jørgensen J. K., Nordlund Å., Moynier F. and Bizzarro M. (2017) Early formation of planetary building blocks inferred from Pb isotopic ages of chondrules. *Sci. Adv.* **3**, e1700407.

Budde G., Kleine T., Kruijer T. S., Burkhardt C. and Metzler K. (2016) Tungsten isotopic constraints on the age and origin of chondrules. *Proc. Natl. Acad. Sci.* **113**, 2886–2891.

Budde G., Kruijer T. S. and Kleine T. (2018) Hf-W chronology of CR chondrites: Implications for the timescales of chondrule formation and the distribution of ^{26}Al in the solar nebula. *Geochim. Cosmochim. Acta* **222**, 284–304.

Cherniak D. J., Lanford W. A. and Ryerson F. J. (1991) Lead diffusion in apatite and zircon using ion implantation and Rutherford backscattering techniques. *Geochim. Cosmochim. Acta* **55**, 1663–1673.

Cherniak D. J. and Van Orman J. A. (2014) Tungsten diffusion in olivine. *Geochim. Cosmochim. Acta* **129**, 1–12.

Cook D. L. and Schönbächler M. (2016) High-precision measurement of W isotopes in Fe–Ni alloy and the effects from the nuclear field shift. *J. Anal. At. Spectrom.* **31**, 1400–1405.

Dodd R. T. (1969) Metamorphism of the ordinary chondrites: a review. *Geochim. Cosmochim. Acta* **33**, 161–203.

Dodd R. T. (1981) *Meteorites: A petrologic-chemical synthesis*. Cambridge University Press, New York.

Eiler J. M., Baumgartner L. P. and Valley J. W. (1992) Intercrystalline stable isotope diffusion: a fast grain boundary model. *Contrib. Mineral. Petrol.* **112**, 543–557.

Ganguly J., Tirone M. and Domanik K. (2016) Cooling rates of LL, L and H chondrites and constraints on the duration of peak thermal conditions: Diffusion kinetic modeling and implications for fragmentation of asteroids and impact resetting of petrologic types. *Geochim. Cosmochim. Acta* **192**, 135–148.

Gastineau-Lyons H. K., McSween H. Y. and Gaffey M. J. (2002) A critical evaluation of oxidation versus reduction during metamorphism of L and LL group chondrites, and implications for asteroid spectroscopy. *Meteorit. Planet. Sci.* **37**, 75–89.

Göpel C., Manhes G. and Allegre C. J. (1994) U-Pb systematics of phosphates from equilibrated ordinary chondrites. *Earth Planet. Sci. Lett.* **121**, 153–171.

Henke S., Gail H.-P., Trieloff M., Schwarz W. H. and Kleine T. (2012) Thermal evolution and sintering of chondritic planetesimals. *Astronomy & Astrophysics* **537**, A45.

Huss G. R., Rubin A. E. and Grossman J. N. (2006) Thermal metamorphism in chondrites. In *Meteorites and the Early Solar System II* (eds. D. S. Lauretta and H. Y. McSween). University of Arizona Press, Tucson, pp. 567–586.

Jacobsen S. B. (2005) The Hf-W isotopic system and the origin of the Earth and Moon. *Annu. Rev. Earth Planet. Sci.* **33**, 531–570.

Jacquet E. (2014) Transport of solids in protoplanetary disks: Comparing meteorites and astrophysical models. *C.R. Geosci.* **346**, 3–12.

Keil K. (2000) Thermal alteration of asteroids: evidence from meteorites. *Planet. Space Sci.* **48**, 887–903.

Kessel R., Beckett J. R. and Stolper E. M. (2007) The thermal history of equilibrated ordinary chondrites and the relationship between textural maturity and temperature. *Geochim. Cosmochim. Acta* **71**, 1855–1881.

Kita N. T., Nagahara H., Togashi S. and Morishita Y. (2000) A short duration of chondrule formation in the solar nebula: Evidence from ^{26}Al in Semarkona ferromagnesian chondrules. *Geochim. Cosmochim. Acta* **64**, 3913–3922.

Kita N. T. and Ushikubo T. (2012) Evolution of protoplanetary disk inferred from ^{26}Al chronology of individual chondrules. *Meteorit. Planet. Sci.* **47**, 1108–1119.

Kleine T., Hans U., Irving A. J. and Bourdon B. (2012) Chronology of the angrite parent body and implications for core formation in protoplanets. *Geochim. Cosmochim. Acta* **84**, 186–203.

Kleine T., Mezger K., Münker C., Palme H. and Bischoff A. (2004) ^{182}Hf-^{182}W isotope systematics of chondrites, eucrites, and martian meteorites: Chronology of core formation and early mantle differentiation in Vesta and Mars. *Geochim. Cosmochim. Acta* **68**, 2935–2946.

Kleine T., Münker C., Mezger K. and Palme H. (2002) Rapid accretion and early core formation on asteroids and the terrestrial planets from Hf-W chronometry. *Nature* **418**, 952–955.

Kleine T., Touboul M., Bourdon B., Nimmo F., Mezger K., Palme H., Jacobsen S. B., Yin Q.-Z. and Halliday A. N. (2009) Hf–W chronology of the accretion and early evolution of asteroids and terrestrial planets. *Geochim. Cosmochim. Acta* **73**, 5150–5188.

Kleine T., Touboul M., Van Orman J. A., Bourdon B., Maden C., Mezger K. and Halliday A. N. (2008) Hf–W thermochronometry: closure temperature and constraints on the accretion and cooling history of the H chondrite parent body. *Earth Planet. Sci. Lett.* **270**, 106–118.

Kleine T. and Walker R. J. (2017) Tungsten isotopes in planets. *Annu. Rev. Earth Planet. Sci.* **45**, 389–417.

Kruijer T., Touboul M., Fischer-Gödde M., Bermingham K., Walker R. and Kleine T. (2014a) Protracted core formation and rapid accretion of protoplanets. *Science* **344**, 1150–1154.

Kruijer T. S., Burkhardt C., Budde G. and Kleine T. (2017) Age of Jupiter inferred from the distinct genetics and formation times of meteorites. *Proc. Natl. Acad. Sci.* **114**, 6712–6716.

Kruijer T. S., Kleine T., Fischer-Gödde M., Burkhardt C. and Wieler R. (2014b) Nucleosynthetic W isotope anomalies and the Hf–W chronometry of Ca–Al-rich inclusions. *Earth Planet. Sci. Lett.* **403**, 317–327.

Kruijer T. S., Sprung P., Kleine T., Leya I., Burkhardt C. and Wieler R. (2012) Hf–W chronometry of core formation in planetesimals inferred from weakly irradiated iron meteorites. *Geochim. Cosmochim. Acta* **99**, 287–304.

Lee D.-C. and Halliday A. N. (2000) Accretion of primitive planetesimals: Hf-W isotopic evidence from enstatite chondrites. *Science* **288**, 1629–1631.

Ludwig K. R. (1991) ISOPLOT: a plotting and regression program for radiogenic isotope data; version 2.53. In *Open-File Report*, 91-445. U.S.Geological Survay.

Pape J., Mezger K., Bouvier A.-S. and Baumgartner L. P. (2019) Time and duration of chondrule formation: Constraints from ^{26}Al-^{26}Mg ages of individual chondrules. *Geochim. Cosmochim. Acta* **244**, 416–436.

Rudraswami N. G. and Goswami J. N. (2007) ^{26}Al in chondrules from unequilibrated L chondrites: Onset and duration of chondrule formation in the early solar system. *Earth Planet. Sci. Lett.* **257**, 231–244.

Scott E. R. D., Krot T. V., Goldstein J. I. and Wakita S. (2014) Thermal and impact history of the H chondrite parent asteroid during metamorphism: Constraints from metallic Fe–Ni. *Geochim. Cosmochim. Acta* **136**, 13–37.

Slater-Reynolds V. and McSween H. Y. (2005) Peak metamorphic temperatures in type 6 ordinary chondrites: An evaluation of pyroxene and plagioclase geothermometry. *Meteorit. Planet. Sci.* **40**, 745–754.

Taylor G. J., Maggiore P., Scott E. R. D., Rubin A. E. and Keil K. (1987) Original structures, and fragmentation and reassembly histories of asteroids: Evidence from meteorites. *Icarus* **69**, 1–13.

Touboul M. and Walker R. J. (2012) High precision tungsten isotope measurement by thermal ionization mass spectrometry. *Int. J. Mass Spectrom.* **309**, 109–117.

Trieloff M., Jessberger E. K., Herrwerth I. and Hopp J. (2003) Structure and thermal history of the H-chondrite parent asteroid revealed by thermochronometry. *Nature* **422**, 502–506.

Van Orman J. A., Grove T. L. and Shimizu N. (2001) Rare earth element diffusion in diopside: influence of temperature, pressure, and ionic radius, and an elastic model for diffusion in silicates. *Contrib. Mineral. Petrol.* **141**, 687–703.

Van Orman J. A., Saal A. E., Bourdon B. and Hauri E. H. (2006) Diffusive fractionation of U-series radionuclides during mantle melting and shallow-level melt–cumulate interaction. *Geochim. Cosmochim. Acta* **70**, 4797–4812.

Villeneuve J., Chaussidon M. and Libourel G. (2009) Homogeneous distribution of 26Al in the solar system from the Mg isotopic composition of chondrules. *Science* **325**, 985–988.

Warren P. H. (2011) Stable-isotopic anomalies and the accretionary assemblage of the Earth and Mars: A subordinate role for carbonaceous chondrites. *Earth Planet. Sci. Lett.* **311**, 93–100.

Willbold M., Elliott T. and Moorbath S. (2011) The tungsten isotopic composition of the Earth's mantle before the terminal bombardment. *Nature* **477**, 195–199.

Worsham E. A., Bermingham K. R. and Walker R. J. (2017) Characterizing cosmochemical materials with genetic affinities to the Earth: Genetic and chronological diversity within the IAB iron meteorite complex. *Earth Planet. Sci. Lett.* **467**, 157–166.

Associate editor: Sara S. Russell